

<sup>1</sup> The effects of multi-dimensional drought on land cover change and  
<sup>2</sup> vegetation productivity in continental Chile

<sup>3</sup> Francisco Zambrano<sup>a,1,\*</sup>, Anton Vrieling<sup>b</sup>, Francisco Meza, Iongel Duran-Llacer, Francisco Fernández<sup>c</sup>,  
<sup>4</sup> Alejandro Venegas-González, Nicolas Raab, Dylan Craven

<sup>a</sup> Universidad Mayor, Hémera Centro de Observación de la Tierra, Facultad de Ciencias, Escuela de Ingeniería en Medio Ambiente y Sustentabilidad, Santiago, Chile, 7500994

<sup>b</sup> University of Twente, Faculty of Geo-Information Science and Earth Observation (ITC), Enschede, The Netherlands,

<sup>c</sup> Universidad San Sebastián,

---

<sup>5</sup> **Abstract**

The north-central region of Chile has been the focus of research studies due to the persistent decrease in water supply, which is impacting the hydrological system and vegetation development. This persistent period of water scarcity has been defined as a megadrought. The aim of our study is to evaluate the land cover change over continental Chile and to examine how this is connected to drought indices of water supply, atmospheric evaporative demand (AED), soil moisture, and their effects on vegetation productivity. The drought indices were derived using monthly ERA5-Land reanalysis data spanning from 1981 to 2023. The Moderate-Resolution Imaging Spectroradiometer (MODIS) datasets were utilized to obtain information on annual land cover and monthly vegetation productivity. We analyzed short- (1, 3, 6 months) to long-term (12, 24, 36 months) time scales of drought. Our results showed that land cover change was highest in the south-central part of the country, reaching changes as high as 36% in the surface type. The water demand has increased for the whole country, with a major increase in the north. The AED and soil moisture evidence a decreasing trend, which decreases at longer time scales and from north to south. The extreme south part of the country shows an increase in supply. Vegetation productivity has a negative trend in the north-central region for all land cover types. On the other hand, forests seem to be the most resistant type to drought. The types that show to be most affected by variation in climate conditions are shrublands, savannas, and croplands. The drought indices that have the capability of explaining to a major degree the variance in vegetation productivity are the ones that consider soil moisture for twelve months and the combined effect of precipitation and AED for 24 and 12 months. The results indicate that the north-central region is the most sensitive to water supply deficits lasting longer than a year.

<sup>6</sup> **Keywords:** drought, land cover change, satellite

---

<sup>7</sup> **1. Introduction**

<sup>8</sup> Drought is often classified as meteorological when there is a decrease in precipitation below the mean  
<sup>9</sup> average of several years (more than 30 years), hydrological when these anomalies last for long periods (months  
<sup>10</sup> to years) and affect water systems, and agricultural when the deficit impacts plant health anomalies and

---

\*Corresponding author

Email addresses: francisco.zambrano@umayor.cl (Francisco Zambrano), a.vrieling@utwente.nl (Anton Vrieling), francisco.fernandez@uss.cl (Francisco Fernández)

<sup>1</sup>This is the first author footnote.

leads to decreased productivity (Wilhite and Glantz, 1985). However, it is important to note that drought is also influenced by human activities, which were not considered in the definitions. Thus, Van Loon et al. (2016) and AghaKouchak et al. (2021) have given an updated definition of drought for the Anthropocene, suggesting that it should be considered the feedback of humans' decisions and activities that drives the anthropogenic drought. Simultaneously, drought leads to heightened tree mortality and induces alterations in land cover and land use, ultimately affecting ecosystems (Crausbay et al., 2017). Even though many ecological studies have misinterpreted how to characterize drought, for example, sometimes considering "dry" conditions as "drought" (Slette et al., 2019). Then, Crausbay et al. (2017) proposed the ecological drought definition as "an episodic deficit in water availability that drives ecosystems beyond thresholds of vulnerability, impacts ecosystem services, and triggers feedback in natural and/or human systems." In light of current global warming, it is crucial to study the interaction between drought and ecosystems in order to understand their feedback and impact on water security. (Bakker, 2012)

Human-induced greenhouse gas emissions have increased the frequency and/or intensity of drought as a result of global warming, according to the sixth assessment report (AR6) of the Intergovernmental Panel on Climate Change (IPCC) (Calvin et al., 2023). The evidence supporting this claim has been strengthened since AR5 (IPCC, 2013). Recent studies, however, have produced contrasting findings, suggesting that drought has not exhibited a significant trend over the past forty years. (Vicente-Serrano et al., 2022; Kogan et al., 2020). Vicente-Serrano et al. (2022) analyzed the meteorological drought trend on a global scale, finding that only in a few regions has there been an increase in the severity of drought. Moreover, they attribute the increase in droughts over the past forty years solely to an increase in atmospheric evaporative demand (AED), which in turn enhances vegetation water demand, with important implications for agricultural and ecological droughts. Also, they state that "the increase in hydrological droughts has been primarily observed in regions with high water demand and land cover change". Similarly, Kogan et al. (2020) analyzed the drought trend using vegetation health methods, finding that for the globe, hemispheres, and main grain-producing countries, drought has not expanded or intensified for the last 38 years. Further, the Masson-Delmotte (2021) suggests that there is a high degree of confidence that rising temperatures will increase the extent, frequency, and severity of droughts. Also, AR6 (Calvin et al., 2023) predicts that many regions of the world will experience more severe agricultural and ecological droughts even if global warming stabilizes at 1.5°–2°C. To better evaluate the impact of drought trends on ecosystems, assessments are needed that relate meteorological and soil moisture variables to their effects on vegetation.

From 1960 to 2019, land use change has impacted around one-third of the Earth's surface, which is four times more than previously thought (Winkler et al., 2021). Multiple studies aim to analyze and forecast changes in land cover globally (Winkler et al., 2021; Song et al., 2018) and regionally (Chamling and Bera, 2020; Homer et al., 2020; Yang and Huang, 2021). Some others seek to analyze the impact of land cover change on climate conditions such as temperature and precipitation (Luyssaert et al., 2014; Pitman et al., 2012). There is less research on the interaction between drought and land cover change (Chen et al., 2022; Akinyemi, 2021; Peng et al., 2017). Peng et al. (2017) conducted a worldwide investigation utilizing net primary production to examine the spatial and temporal variations in vegetation productivity at global level. The study aimed to assess the influence of drought by comparing the twelve-month Standardized Precipitation Evapotranspiration Index (SPEI) and land cover change. According to their findings, drought is responsible for 37% of the decline in vegetation productivity, while water availability accounts for 55% of the variation. Chen et al. (2022) studied the trend of vegetation greenness and productivity and its relation to meteorological drought (SPEI of twelve months in December) and soil moisture at the global level. The results showed lower correlations (<0.2) for both variables. Akinyemi (2021) evaluates drought trends and land cover change using vegetation indices in Botswana in a semi-arid climate. These studies mostly looked at how changes in land cover and vegetation productivity are related to a single drought index (SPEI) over a single time period of 12 months. SPEI takes into account the combined effect of precipitation and AED as a water balance, but it does not allow us to know the contribution of each variable on its own. Some things worth investigating in terms of land cover change and vegetation productivity are: i) How do they respond to short- to long-term meteorological and soil moisture droughts? ii) How is the drought impacting land cover changes? And iii) How do they behave in humid and arid climatic zones regarding drought? Likewise,

62 there is a lack of understanding of how the alteration in water supply and demand is affecting land cover  
63 transformations.

64 For monitoring drought, the World Meteorological Organization recommends the SPI (Standardized Pre-  
65 cipitation Index) ([WMO et al., 2012](#)). The SPI is a multi-scalar drought index that only uses precipitation  
66 to assess short- to long-term droughts. The primary cause of drought is precipitation anomalies, and tem-  
67 perature usually makes it worse ([Luo et al., 2017](#)). Nowadays, there is an increase in attention toward  
68 using AED separately to monitor droughts ([Vicente-Serrano et al., 2020](#)). One reason is due to its attri-  
69 bution to increasing flash droughts in water-limited regions ([Noguera et al., 2022](#)). [Vicente-Serrano et al.](#)  
70 ([2010](#)) proposed the Standardized Precipitation Evapotranspiration Index (SPEI), which incorporated the  
71 temperature effect by subtracting AED from precipitation. SPEI allows for analysis of the combined effect  
72 of precipitation and AED. Since its formulation, it has been used worldwide for the study and monitoring  
73 of drought ([Gebrechorkos et al., 2023](#); [Liu et al., 2024](#)). [Hobbins et al. \(2016\)](#) and [McEvoy et al. \(2016\)](#)  
74 developed the Evaporative Demand Drought Index (EDDI) to monitor droughts solely using the AED, and  
75 it has proven effective in monitoring flash droughts ([Li et al., 2024](#); [Ford et al., 2023](#)). For soil moisture,  
76 several drought indices exist, such as the Soil Moisture Deficit Index (SDMI) ([Narasimhan and Srinivasan,](#)  
77 [2005](#)) and the Soil Moisture Agricultural Drought Index (SMADI) ([Souza et al., 2021](#)). [Hao and AghaK-](#)  
78 [ouchak \(2013\)](#) and [AghaKouchak \(2014\)](#) proposed the Standardized Soil Moisture Index (SSI), which has  
79 a similar formulation as the SPI, SPEI, and EDDI. Thus, there are plenty of drought indices that allow  
80 for a comprehensive assessment of drought from short- to long-term scales and consider variables from the  
81 earth's water balance on their own (e.g., precipitation, AED, soil moisture). Using this information, we can  
82 advance our understanding of the impact of drought on ecosystems.

83 Chile's diverse climatic and ecosystem types ([Beck et al., 2023](#); [Luebert and Pliscoff, 2022](#)) make it an  
84 ideal natural laboratory for studying climate and ecosystems. Additionally, the country has experienced  
85 severe drought conditions that have had significant effects on vegetation and water storage. North-central  
86 Chile has faced a persistent precipitation deficit since 2010, defined as a mega drought. ([Garreaud et al.,](#)  
87 [2017](#)), which has impacted the Chilean ecosystem. This megadrought was defined by the Standardized  
88 Precipitation Index (SPI) of twelve months in December having values below one standard deviation. Some  
89 studies have addressed how this drought affects single ecosystems in terms of forest development ([Miranda](#)  
90 [et al., 2020](#); [Venegas-González et al., 2018](#)), forest fire occurrence ([Urrutia-Jalabert et al., 2018](#)), and crop  
91 productivity ([Zambrano, 2023](#); [Zambrano et al., 2018, 2016](#)). We found one study regarding land cover and  
92 drought in Chile. The study by [Fuentes et al. \(2021\)](#) evaluates water scarcity and land cover change in Chile  
93 between 29° and 39° of south latitude. [Fuentes et al. \(2021\)](#) used the SPEI of one month for evaluating  
94 drought, which led to misleading results. For example, they did not find a temporal trend in the SPEI but  
95 found a decreasing trend in water availability and an increase trend on AED, which in turn should have  
96 been capable of being captured with longer time scales of the SPEI. The term "megadrought" in Chile is  
97 used to describe a prolonged water shortage that lasts for several years, resulting in a permanent deficit  
98 that impacts the hydrological system ([Boisier et al., 2018](#)). Therefore, it is crucial to evaluate temporal  
99 scales that consider the cumulative impact over a period of several years. There is limited understanding  
100 of the correlation between drought and the environment in Chile. Therefore, it is crucial to have a deeper  
101 understanding of how meteorological and soil moisture droughts impact the dynamics of the environment  
102 in order to make informed decisions on how to adapt.

103 Here, we analyze the multi-dimensional impacts of drought across ecosystems in continental Chile. More  
104 specifically, we aim to assess: i) short- to long-term temporal trends in multi-scalar drought indices; ii)  
105 temporal changes in land-use cover and the direction and magnitude of their relationships with trends in  
106 drought indices; and iii) the trend in vegetation productivity and its relationship with drought indices across  
107 Chilean ecosystems.

108 **2. Study area**

109 Continental Chile has diverse climate conditions with strong gradients from north to south and east to west  
110 ([Aceituno et al., 2021](#)) (Figure 1 a), which determines its great ecosystem diversity ([Luebert and Pliscoff,](#)  
111 [2022](#)) (Figure 1 c). The Andes Mountains are a main factor in climate latitudinal variation ([Garreaud, 2009](#)).  
112 “Norte Grande” and “Norte Chico” predominate in an arid desert climate with hot (Bwh) and cold (Bwk)  
113 temperatures. At the south of “Norte Chico,” the climate changes to an arid steppe with cold temperatures  
114 (Bsk). In these two northern regions, the land is mostly bare, with a small surface of vegetation types  
115 such as shrubland and grassland. In the zones “Centro” and the north half of “Sur,” the main climate is  
116 Mediterranean, with warm to hot summers (Csa and Csb). Land cover in “Centro” comprises a significant  
117 amount of shrubland and savanna (50%), grassland (16%), forest (8%), and croplands (5%). An oceanic  
118 climate (Cfb) predominates in the south of “Sur” and the north of “Austral.” Those zones are high in forest  
119 and grassland. The southern part of the country has a tundra climate, and in “Austral,” it is a cold semi-arid  
120 area with an extended surface of grassland, forest, and, to a lesser extent, savanna.

121 **3. Materials and Methods**

122 *3.1. Data*

123 *3.1.1. Gridded meteorological and vegetation data*

124 To analyze land cover change, we use the classification scheme by the IGBP (International Geosphere-  
125 Biosphere Programme) from the product MCD12Q1 collection 6.1 from MODIS. To derive a proxy for vegeta-  
126 tion productivity, we used the Normalized Difference Vegetation Index (NDVI) from the product MOD13A3  
127 collection 6.1 from MODIS ([Didan, 2015](#)). MOD13A3 provides vegetation indices at 1km of spatial resolution  
128 and monthly frequency. The NASA EOSDIS Land Processes Distributed Active Archive Center (LP DAAC),  
129 USGS Earth Resources Observation and Science (EROS) Center, Sioux Falls, South Dakota, provided the  
130 MOD13A3 and MCD12Q1 from the online Data Pool, accessible at <https://lpdaac.usgs.gov/tools/data-pool/>.

Table 1: Description of the satellite and reanalysis data used

Product	Sub-product	Variable	Spatial Resolution	Period	Units	Short Name
ERA5L		Precipitation	0.1°	1981-2023	mm	P
		Maximum temperature			°C	$T_{max}$
		Minimum temperature			°C	$T_{min}$
		Volumetric Soil Water Content at 1m			m3/m3	SM
ERA5L*	MOD13A3.061	Atmospheric Evaporative Demand	0.1°	1981-2023	mm	AED
MODIS		Normalized Difference Vegetation Index	1 km	2000-2023		NDVI
		land cover IGBP scheme		2001-2022		land cover

\*Calculated from maximum and minimum temperatures derived from ERA5L with Eq. 1.

131 For soil moisture, water supply, and water demand variables, we used ERA5L (ECMWF Reanalysis version  
132 5 over land) ([Muñoz-Sabater et al., 2021](#)), a reanalysis dataset that provides the evolution of atmospheric and  
133 land variables since 1950. It has a spatial resolution of 0.1° (9 km), hourly frequency, and global coverage.  
134 We selected the variables for total precipitation, maximum and minimum temperature at 2 meters, and  
135 volumetric soil water layers between 0 and 100cm of depth (layer 1 to layer 3). Table 1 shows a summary  
136 of the data and its main characteristics.

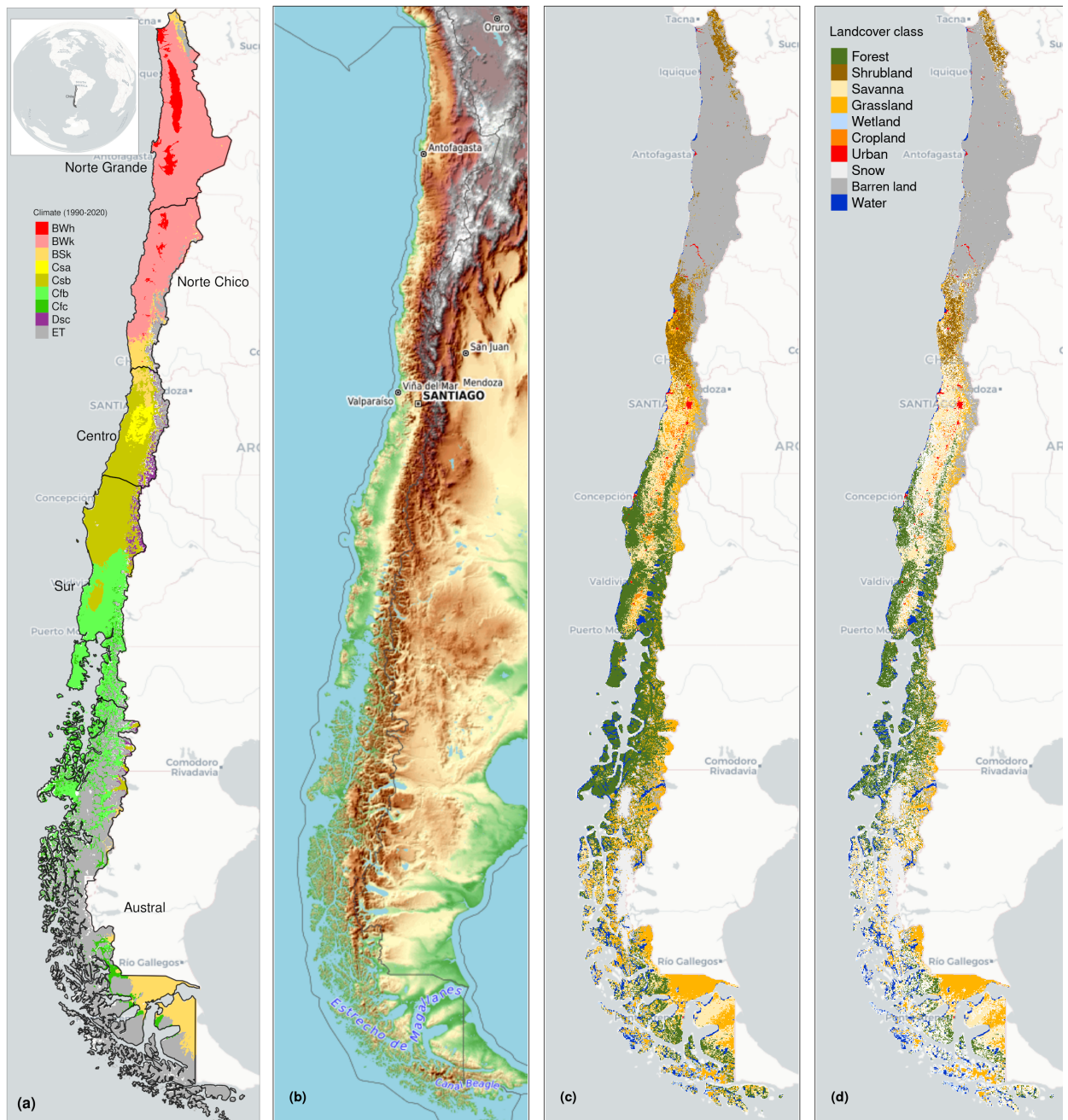


Figure 1: (a) Chile with the Koppen-Geiger climate classes and the five macrozones “Norte Grande”, “Norte Chico”, “Centro”, “Sur”, and “Austral”. (b) Topography reference map. (c) land cover classes for 2022. (d) Persistent land cover classes (> 80%) for 2001-2022

137 *3.2. Trend of short- to long-term drought*

138 *3.2.1. Atmospheric Evaporative Demand (AED)*

139 In order to compute the drought indices that use water demand, it is necessary to first calculate the  
140 AED. To do this, we employed the Hargreaves method ([Hargreaves, 1994](#); [Hargreaves and Samani, 1985](#)) by

141 applying the following equation:

$$AED = 0.0023 \cdot Ra \cdot (T + 17.8) \cdot (T_{max} - T_{min})^{0.5} \quad (1)$$

142 where  $Ra$  ( $MJ\ m^2\ day^{-1}$ ) is extraterrestrial radiation;  $T$ ,  $T_{max}$ , and  $T_{min}$  are mean, maximum, and  
143 minimum temperature ( $^{\circ}C$ ) at 2m. For calculating  $Ra$  we used the coordinate of the latitud of the centroid  
144 of each pixel. We chose the method of Hargreaves to estimate AED because of its simplicity, which only  
145 requires temperatures and extrarrestrial radiation. Also, it has been recommended over other methods (e.g.,  
146 Penman-Monteith) when the access to climatic variables is limited (Vicente-Serrano et al., 2014).

### 147 3.2.2. Non-parametric calculation of drought indices

148 To derive the drought indices of water supply and demand, soil moisture, and vegetation (i.e., the proxy of  
149 productivity), we used the ERA5L dataset and the MODIS product, with a monthly frequency for 1981–2023  
150 and 2000–2023, respectively.

151 The drought indices correspond to a historical anomaly with regard to a variable (e.g., meteorological,  
152 vegetation, or soil moisture). To account for the anomaly, the common practice is to derive it following  
153 a statistical parametric methodology in which it is assumed that the statistical distribution of the data is  
154 known (Heim (2002)). A wrong decision is usually the highest source of uncertainty (Laimighofer and Laaha  
155 (2022)). In the case of Chile, due to its high degree of climatic variability, it is complex to choose a proper  
156 distribution without previous research. Here, we follow a non-parametric methodology for the calculation  
157 of the drought indices, in a similar manner as the framework proposed by Farahmand and AghaKouchak  
158 (2015); Hobbins et al. (2016); McEvoy et al. (2016).

159 For the purpose of monitoring water supply drought, we used the well-known Standardized Precipitation  
160 Index (SPI), which the World Meteorological Organization (WMO) recommended. The SPI solely relies on  
161 precipitation data. Also, it has been used worldwide for the study of drought, including in Chile (Garreaud  
162 et al. (2017); Zambrano et al. (2017)). The primary cause of drought is precipitation anomalies, and  
163 temperature usually makes it worse (Luo et al., 2017). Nowadays, there is an increase in attention toward  
164 using water demand separately to monitor droughts. (Vicente-Serrano et al. (2020); Noguera et al. (2022)).  
165 Thus, to evaluate water demand, we chose the Evaporative Demand Drought Index (EDDI), developed by  
166 Hobbins et al. (2016) and McEvoy et al. (2016), which is based on the AED. EDDI is currently used for  
167 monitoring drought in the United States (<https://psl.noaa.gov/eddi/>). In our case, we used only temperature  
168 for AED, a difference from the original formulation of EDDI, which also considered wind besides temperature.  
169 To consider the combined effect of water supply and demand, we selected the SPEI, which corresponds to  
170 a balance between precipitation and AED. Vicente-Serrano et al. (2010) proposed the SPEI, and it has  
171 improved the SPI by incorporating temperature for drought monitoring. For SPEI, an auxiliary variable  $D$   
172 =  $P$ -AED is calculated. Soil moisture is the main driver of vegetation productivity, particularly in semi-arid  
173 regions (Li et al. (2022)). Hence, for soil water drought, we used the SSI (Standardized Soil Moisture Index)  
174 (Hao and AghaKouchak, 2013; AghaKouchak, 2014) which is a multi-scale index similar to SPI, SPEI, and  
175 EDDI. In our case, for the SSI, we used the average soil moisture from ERA5L at 1m depth. Finally, for  
176 the proxy of productivity, we used the zcNDVI proposed by Zambrano et al. (2018) which will be derived  
177 from the NDVI retrieved from MOD13A1.

178 To derive the drought indices, first we must calculate the sum of the variables with regard to the time scale  
179 ( $s$ ). In this case, for generalization purposes, we will use  $V$ , referring to variables  $P$ ,  $AED$ ,  $D$ ,  $NDVI$ , and  
180  $SM$  (Table 1). We cumulated each  $V$  over the time series of  $n$  values (months), and for the time scales  $s$ :

$$A_{si} = \sum_{i=n-s-i+2}^{n-i+1} V_i \quad \forall i \geq n-s+1 \quad (2)$$

181 The  $A_{si}$  corresponds to a moving window (convolution) that sums the variable for time scales  $s$  from the  
 182 last month, month by month, until the first month in which it could sum for  $s$  months. Once the variable  
 183 is cumulated over time for the scale  $s$ . Thus, the empirically derived probabilities are obtained through an  
 184 inverse normal approximation (Abramowitz and Stegun, 1968). Then, we used the empirical Tukey plotting  
 185 position (Wilks, 2011) over  $A_i$  to derive the  $P(a_i)$  probabilities across a period of interest:

$$P(A_i) = \frac{i - 0.33}{n + 0.33} \quad (3)$$

186 The drought indices *SPI*, *SPEI*, *EDDI*, *SSI*, and *zcNDVI* are obtained following the inverse normal  
 187 approximation:

$$DI(A_i) = W - \frac{C_0 + C_1 \cdot W + c_2 \cdot W^2}{1 + d_1 \cdot W + d_2 \cdot W^2 + d_3 \cdot W^3} \quad (4)$$

188  $DI$  is referring to the drought index calculated for the variable  $V$ . The values for the constats are:  
 189  $C_0 = 2.515517$ ,  $C_1 = 0.802853$ ,  $C_2 = 0.010328$ ,  $d_1 = 1.432788$ ,  $d_2 = 0.189269$ , and  $d_3 = 0.001308$ . For  
 190  $P(A) \leq 0.5$ ,  $W = \sqrt{-2 \cdot \ln(P(A_i))}$ , and for  $P(A_i) > 0.5$ , replace  $P(A_i)$  with  $1 - P(A_i)$  and reverse the sign  
 191 of  $DI(A_i)$ .

192 The drought indices were calculated for time scales of 1, 3, 6, 12, 24, and 36 months at a monthly frequency  
 193 for 1981–2023 in order to be used for short- to long-term evaluation of drought. In the case of the proxy of  
 194 vegetation productivity (*zcNDVI*) it was calculated for a time scale of six months at monthly frequency for  
 195 2000–2023. For *zcNDVI*, we test time scales of 1, 3, 6, and 12 months; we choose to use six months because  
 196 that shows a more robust representation of vegetation productivity due to the seasonality of vegetation in  
 197 Chile.

### 198 3.2.3. Trend of drought indices

199 To estimate if there are significant positive or negative trends for the drought indices, we used the non-  
 200 parametric test of Mann-Kendall (Kendall, 1975). To determine the magnitude of the trend, we used Sen's  
 201 slope (Sen, 1968). Some of the advantages of applying this methodology are that the Sen's slope is not  
 202 affected by outliers as regular regression does, and it is a non-parametric method that is not influenced by  
 203 the distribution of the data. We applied Mann-Kendall to see if the trend was significant and Sen's slope  
 204 to estimate the magnitude of the trend. We did this to the six time scales from 1981 to 2023 (monthly  
 205 frequency) and the indices SPI, EDDI, SPEI, and SSI. Thus, we have trends per index and time scale (24 in  
 206 total). Then, we extracted the trend aggregated by macrozone and per land cover persistent macroclasses.

### 207 3.3. Interaction of land cover and drought

#### 208 3.3.1. Land cover change

209 To analyze the land cover change, we use the IGBP scheme from the MCD12Q1 collection 6.1 from MODIS.  
 210 Zambrano et al. (2018) and Fuentes et al. (2021) have previously used this product for studies of drought  
 211 and land cover in Chile. The MCD12Q1 has a yearly frequency from 2001 to 2022. The IGBP defines 17  
 212 classes; from these, we regrouped into ten macroclasses, as follows: classes 1-4 to forest, 5-7 to shrublands,  
 213 8-9 to savannas, 10 as grasslands, 11 as wetlands, 12 and 14 to croplands, 13 as urban, 15 as snow and ice, 16  
 214 as barren, and 17 to water bodies. Thus, we have a land cover raster time series with the ten macroclasses  
 215 for 2001 and 2023. We validate the land cover macroclasses regarding a highly detailed (30 m of spatial  
 216 resolution) land cover map made for Chile by Zhao et al. (2016) for 2013-2014. Our results showed a global  
 217 accuracy of ~0.82 and a F1 score of ~0.66. Section S2 in the Supplementary Material shows the procedure  
 218 for validation.

219 Climate, vegetation development, seasonality, and changes in vegetation type all have an impact on the  
220 time series of NDVI. In this study, we want to examine the variation in vegetation productivity across  
221 various land cover types and how water demand, water supply, and soil moisture affect it. In order to avoid  
222 changes due to a change in the land cover type that will wrongly impact NDVI, we developed a persistence  
223 mask for land cover for 2001–2022. Thereby, we reduce an important source of variation on a regional  
224 scale. Therefore, we generated a raster mask for IGBP MODIS per pixel using macroclasses that remained  
225 unchanged for at least 80% of the years (2001–2022). This enabled us to identify regions where the land  
226 cover macroclasses are persistent. We calculated the surface occupied per land cover class into the five  
227 macrozones (“Norte Grande” to “Austral”) per year for 2001–2023. After that, we calculated the trend’s  
228 change in surface per type. We used the Sen’ slope ([Sen, 1968](#)) based on Mann-Kendall ([Kendall, 1975](#)).

### 229 *3.3.2. Relationship between land cover and drought trends*

230 We wanted to explore the relationship between the trend in land cover classes and the trend in the drought  
231 indices. For this purpose, in order to have more representative results, we conducted the analysis over sub-  
232 basins within continental Chile. We use 469 basins, which have a surface area between 0.0746 and 24,000  
233 ( $km^2$ ), and a median area of 1,249 ( $km^2$ ). For each basin, we calculate the relative trend per land cover  
234 type, considering the proportion of the type relative to the total surface of the basin. Then, we extracted  
235 per basin the average trend of the drought indices SPI, SPEI, EDDI, SSI, and all their time scales 1, 3, 6,  
236 12, 24, and 36. Also, we extracted the average trend in the proxy of vegetation productivity (zcNDVI). We  
237 wanted to analyze which drought indices and time scales have a major impact on changes in land cover type.

238 We have 25 predictors, which are drought indices and vegetation productivity. We analyzed the 25 predictors  
239 per type of landcover. For the analysis, we selected the method of random forest ([Ho \(1995\)](#)). Because  
240 it allows to find no linear relationship, it reduces overfitting and can derive the feature importance, which  
241 helps for a better understanding of the relationships. The importance of the variable is calculated by per-  
242 muting out-of-bag (OOB) data per tree and calculating the mean standard error in the OOB. Then the  
243 same is done after permuting each predictor variable. Random forest uses multiple decision trees and allows  
244 for classification and regression.

245 We analyzed the 25 predictors per type of landcover, thus running six models. We used random forests for  
246 regression and trained 1000 forests. For more reliable results for the important variables, we resampled by  
247 creating ten folds, running a random forest per fold, and calculating the r-squared (rsq), root mean square  
248 error (RMSE), and variable importance ten times.

### 249 *3.4. Drought impacts on vegetation productivity*

250 We analyzed the trend of vegetation productivity over the unchanged land cover macroclasses. This way,  
251 we tried to reduce the noise in the vegetation due to a change in land cover from year to year. To achieve  
252 this, we will use the persistent mask of land cover macroclasses, which are the types that remain more than  
253 80% of the time for 2001–2022. We used this to evaluate the trend in zcNDVI per land cover class and  
254 macrozone.

255 We examine the drought indices of water demand, water supply, soil moisture, and their connection with  
256 vegetation productivity to investigate two main questions: i) whether short-term or long-term time scales  
257 have a greater impact on vegetation across Chile and its specific regions; and ii) the spatial variation  
258 in the strength of the correlation between the variables and time scales. Then, we will summarize for  
259 each land cover class and macrozone. Thus, we will be able to advance in understanding how climate  
260 is affecting vegetation, considering the impact on the five macroclasses of vegetation: forest, cropland,  
261 grassland, savanna, and shrubland.

262 We conducted an analysis on the linear correlation between the indices SPI, SPEI, EDDI, and SSI over  
263 time periods of 1, 3, 6, 12, 24, and 36 months, and zcNDVI. The objective is to determine the impact of  
264 soil moisture and water demand and supply on vegetation productivity. We used a method similar to that

265 used by [Meroni et al. \(2017\)](#) which compared the SPI with the cumulative FAPAR (Fraction of Absorbed  
266 Photosynthetically Active Radiation). A pixel-to-pixel linear correlation analysis was performed for each  
267 index within the persistent mask of land cover macroclasses. To begin, the Pearson coefficient of correlation  
268 is computed for each of the six time scales. A significant time scale is identified as the one that attains the  
269 highest correlation ( $p < 0.05$ ). Subsequently, the Pearson correlation coefficient corresponding to the time  
270 scales at which the value peaked was extracted. As a result, for each index, we generated two raster maps:  
271 1) containing the raster with values of the time scales that reached the maximum correlation, and 2) having  
272 the value of the correlation obtained.

273 *3.5. Software*

274 For the downloading, processing, and analysis of the spatio-temporal data, we used the open source software  
275 for statistical computing and graphics, R ([R Core Team, 2023](#)). For downloading ERA5L, we used the  
276 `{ecmwfr}` package ([Hufkens et al., 2019](#)). For processing raster data, we used `{terra}` ([Hijmans, 2023](#))  
277 and `{stars}` ([Pebesma and Bivand, 2023](#)). For managing vectorial data, we used `{sf}` ([Pebesma, 2018](#)).  
278 For the calculation of AED, we used `{SPEI}` ([Beguería and Vicente-Serrano, 2023](#)). For mapping, we use  
279 `{tmap}` ([Tennekes, 2018](#)). For data analysis, the suite `{tidyverse}` ([Wickham et al., 2019](#)) was used. For  
280 the random forest modeling we used the `{tidymodels}` ([Kuhn and Wickham, 2020](#)) and `{ranger}` ([Wright and  
281 Ziegler, 2017](#)) packages.

282 **4. Results**

283 *4.1. Trend of short- to long-term drought*

284 Figure 2 shows the spatial variation of the trend for the drought indices from short- to long-term scales.  
285 SPI and SPEI have a decreasing trend from “Norte Chico” to “Sur.” However, there is an increasing trend  
286 in “Austral.” The degree of the trend is stronger at higher time scales. The SSI indicates that in “Norte  
287 Grande,” there are surfaces that have increased in the southwest part and in the northeast have decreased,  
288 and is shown for all time scales. Similar to SPI and SPEI, SSI decreases at higher time scales. EDDI showed  
289 a positive trend for the whole of continental Chile, with a higher trend toward the north and a descending  
290 gradient toward the south. The degree of trend increases at higher time scales.

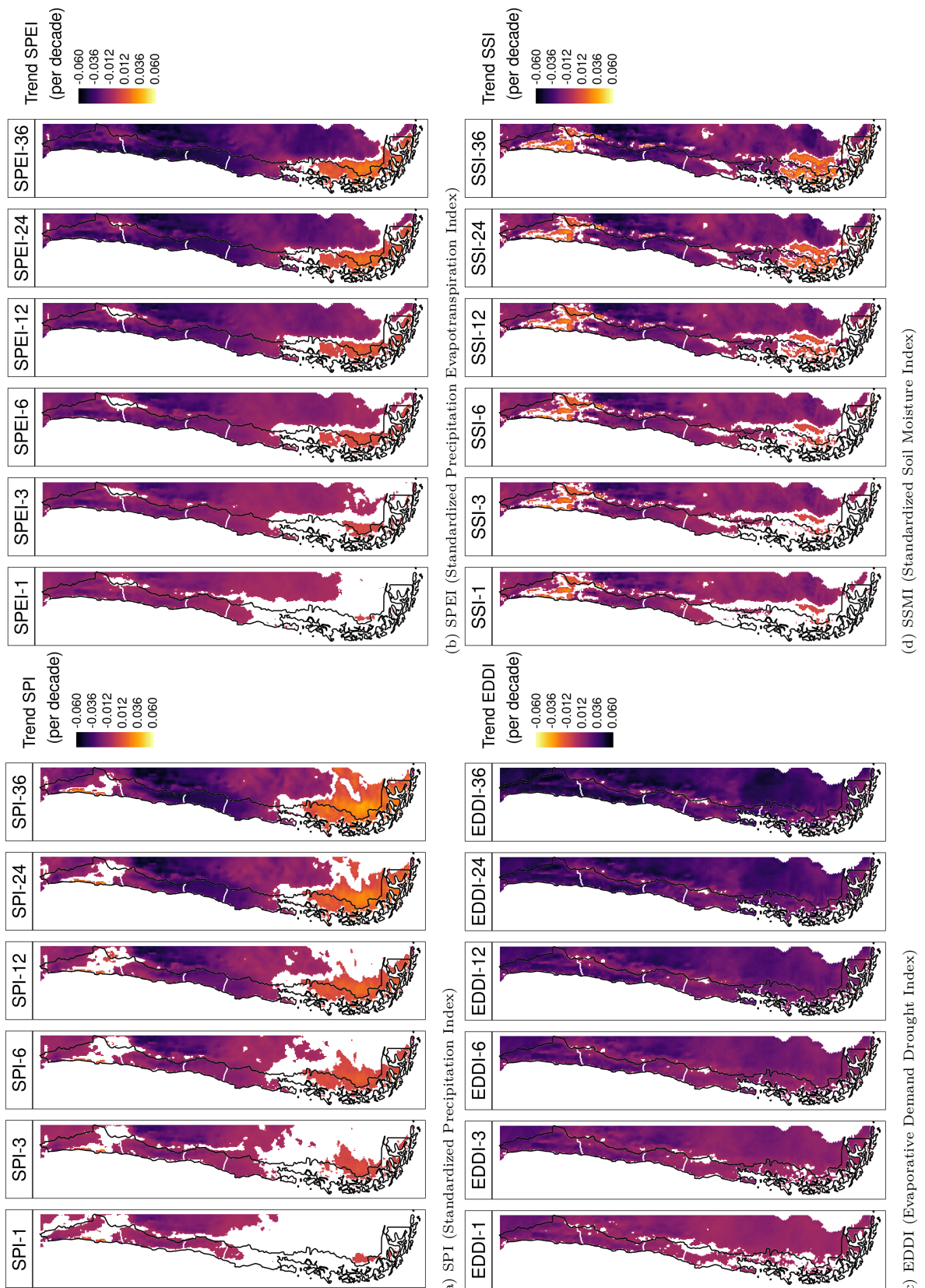


Figure 2: Linear trend of the drought index (\*) at time scales of 1, 3, 6, 12, 24, and 36 months for 1981-2023

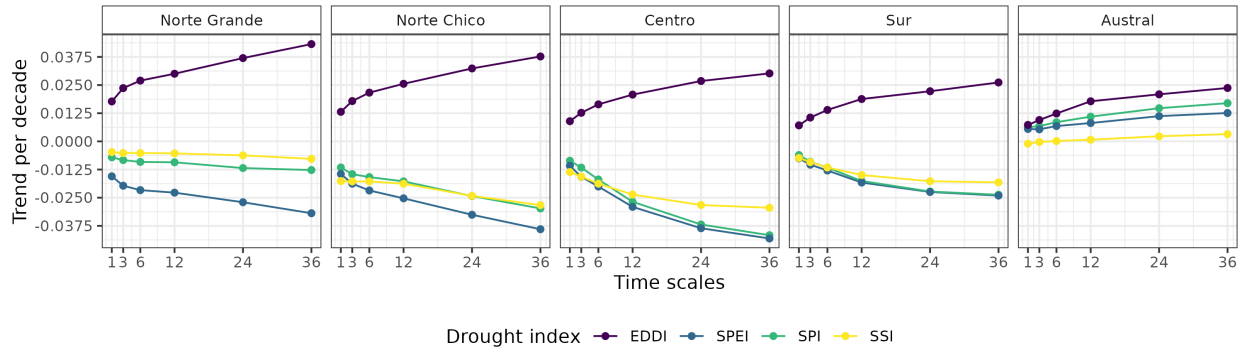


Figure 3: Trend per decade for the drought indices SPI, EDDI, SPEI, and SSI aggregated by macrozone.

In Figure 3, the averaged aggregation per macrozone, drought index, and time scale are shown. The macrozones that have the lowest trend are “Norte Chico” and “Centro,” where the SPI, SPEI, and SSI show that it decreases at longer time scales. Potentially explained due to the prolonged reduction in precipitation that has affected the hydrological system in Chile. At 36 months, it reaches trends between -0.03 and -0.04 (z-score) per decade for SPI, SPEI, and SSI. For “Sur,” the behavior is similar, decreasing at longer scales and having between -0.016 and -0.025 per decade for SPI, SPEI, and SSI. “Norte Grande” has the highest trend at 36 months for EDDI (0.042 per decade), and “Centro” has the lowest for SPI and SPEI. In “Norte Grande” and “Norte Chico,” which are in a semi-arid climate, it is evident that the EDDI has an effect on the difference between the SPI and SPEI index, which is not seen in the other macrozones. Contrary to the other macrozones, “Austral” showed an increase in all indices, being the highest for EDDI at 36 months (0.025) and the lowest for SSI, which shows only a minor increase in the trend.

#### 4.1.1. Interaction of land cover and drought

#### 4.2. Land cover change

Table 2: Surface of the land cover class that persist during 2001-2022

macrozone	Surface [km <sup>2</sup> ]					
	Forest	Cropland	Grassland	Savanna	Shrubland	Barren land
Norte Grande			886		7,910	171,720
Norte Chico		90	4,283	589	16,321	84,274
Centro	3,739	1,904	7,584	19,705	844	12,484
Sur	72,995	1,151	7,198	15,906		2,175
Austral	60,351		54,297	19,007	249	7,218
Total	—	137,085	3,145	74,247	55,206	25,341
						277,870

For vegetation, we obtained and use hereafter five macroclasses of land cover from IGBP MODIS: forest, shrubland, savanna, grassland, and croplands. Figure 1c shows the spatial distribution of the macroclasses through Chile for the year 2022. Figure 1d shows the macroclasses of land cover persistence (80%) during 2021–2022, respectively (Table 2). Within continental Chile, barren land is the land cover class with the highest surface area (277,870 km<sup>2</sup>). The largest type of vegetation, with 137,085 km<sup>2</sup>, is forest. Grassland (74,247 km<sup>2</sup>), savanna (55,206 km<sup>2</sup>), shrubland (25,341 km<sup>2</sup>), and cropland (3,146 km<sup>2</sup>) are the other types (Table 2). The macrozones with major changes for 2001–2022 were “Centro,” “Sur,” and “Austral,” with 36%, 31%, and 34% of their surface changing the type of land cover, respectively (Figure 1 and Table 3). Figure 4 shows the summary of the proportion of surface per land cover class and macrozone, derived from the persistence mask over continental Chile.

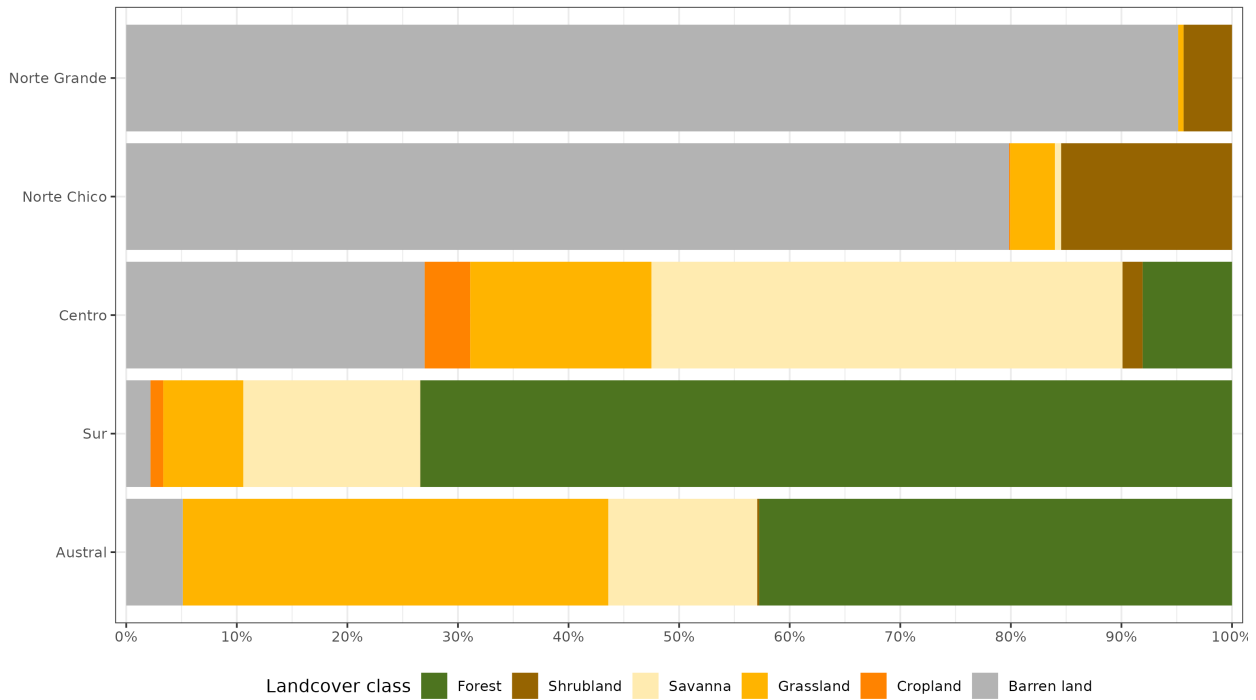


Figure 4: Proportion of land cover class from the persistent land cover for 2001-2022 (>80%) per macrozone

Table 3: The value of Sen's slope trend next to the time-series plot of surface per land cover class (IGBP MCD12Q1.016) for 2001–2022 through Central Chile. Values of zero indicate that there was not a significant trend. Red dots on the plots indicate the maximum and minimum values of surface.

macrozone	Trend of change [km <sup>2</sup> year <sup>-1</sup> ]											
	Forest		Cropland		Grassland		Savanna		Shrubland		Barren land	
	x	y	x	y	x	y	x	y	x	y	x	y
Norte Grande							0.0				0.0	
Norte Chico					-12.1		0.0		-70.0		0.0	111.2
Centro					-22.4		83.2		-136.2		146.0	22.9
Sur		396.6		37.8		0.0		-318.8		172.1		-93.2
Austral		0.0					0.0			-36.9		

314 The “Norte Chico” shows an increase in barren land of  $111 \text{ km}^2 \text{yr}^{-1}$  and a reduction in the class savanna  
 315 of  $70 \text{ km}^2 \text{yr}^{-1}$ . In the “Centro” and “Sur,” there are changes with an important reduction in savanna (136  
 316 to  $318 \text{ km}^2 \text{yr}^{-1}$  ), and an increase in shrubland and grassland. Showing a change for more dense vegetation  
 317 types. It appears to be a shift in the area cultivated (croplands) from the “Centro” to the “Sur.” Also, there  
 318 is a high increase in forest ( $397 \text{ km}^2 \text{yr}^{-1}$  ) in the “Sur,” replacing the savanna lost (Table 3).

#### 319 4.2.1. Relationship between drought indices and land cover change

320 According to Table 4, the trends in drought indices reach an r-squared between 0.32 and 0.39 for the  
 321 types of forest, grassland, savanna, shrubland, and barren land. It is more likely that short- and medium-  
 322 term increases in AED (EDDI-6 and EDDI-12) and short-term precipitation deficits (SPI-6 and SPEI-6)  
 323 contributed to changes in grassland and bare land. The short-term increase of AED (EDDI-3 and EDDI-6)

324 and the longer duration of the precipitation deficit (SPI-24, SPI-36, and SPEI-36) most likely contribute to  
 325 the changes in shrubland. The changes in savanna are associated with a short- and long-term increase in  
 326 AED and a three-year precipitation deficit (SPI-36). The increase in cumulative AED from 12 to 36 months  
 327 is the strongest associated variable that contributes to changes in forests, followed by the reduction of soil  
 328 moisture over six and 36 months. More details about the results of the variable importance can be found in  
 329 the supplementary material in Section S3.

Table 4: The five most important trends of drought indices in estimating the landcover trend per land cover type and the r-squared (rsq) reached by each random forest model.

Position	Forest (rsq=0.32)	Cropland (rsq=0.06)	Grassland (rsq=0.39)	Savanna (rsq=0.23)	Shrubland (rsq=0.23)	Barren_land (rsq=0.32)
1	EDDI-36	EDDI-36	EDDI-6	EDDI-6	EDDI-6	EDDI-12
2	EDDI-24	SSI-36	EDDI-12	EDDI-12	SPI-36	EDDI-6
3	EDDI-12	EDDI-24	EDDI-24	SPI-36	SPEI-36	SPI-6
4	SSI-36	EDDI-12	SPEI-6	EDDI-36	EDDI-3	SPEI-6
5	SSI-6	SSI-24	SPI-6	EDDI-24	SPI-24	EDDI-24

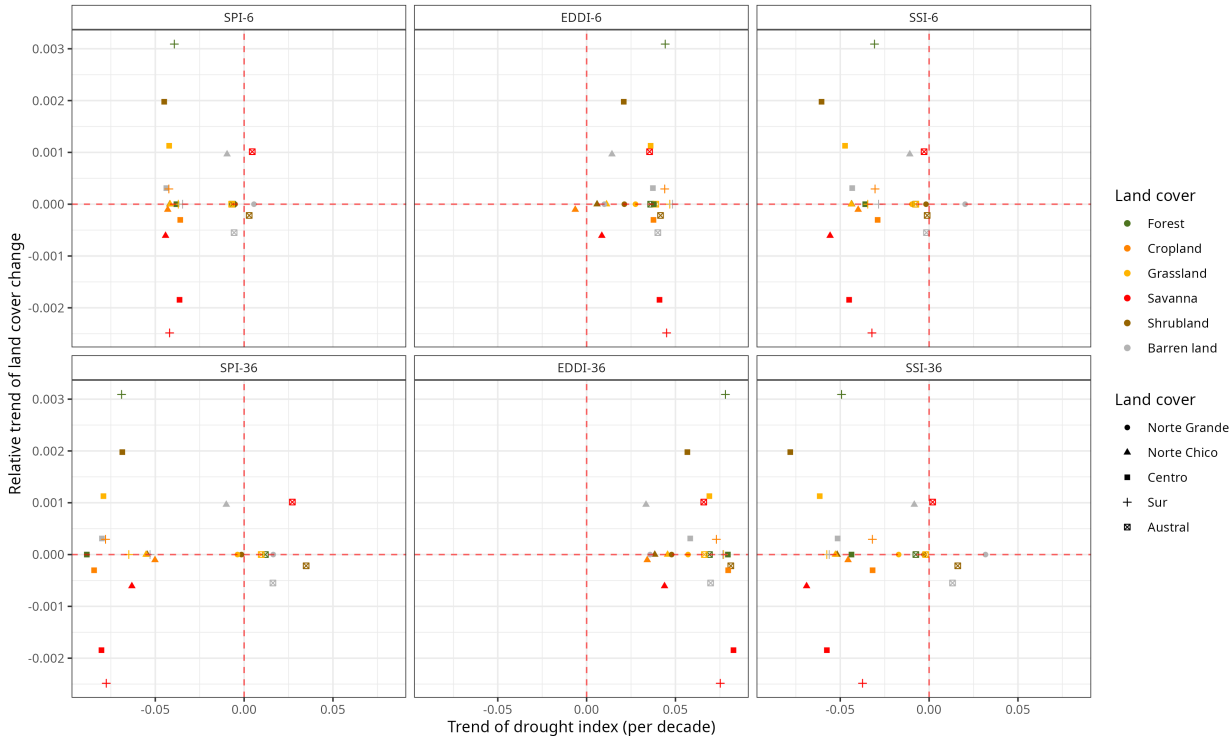


Figure 5: Relationship between the trend in land cover change (y-axis) and the trend in drought indices (x-axis) for the five macrozones. Vertical panels correspond to 1, 3, 6, 12, 24, and 36 months of the time scale by drought index. Horizontal panels show each drought index

330 We study the connection between the SPI, EDDI, and SSI drought indices and changes in land cover in  
 331 Figure 5. To do this, we compare the relative changes in land cover (in terms of the total surface area per  
 332 land cover type and macrozone) over six and thirty-six months. Figure 5 shows that the forest in the “Sur,”

333 shrubland and grassland in “Centro,” barren land in “Norte Chico,” and savanna in “Austral” showed an  
 334 increase in the surface of landcover associated with an increase in EDDI. Savanna in “Centro,” “Sur,” and  
 335 “Norte Chico” decreases with the increase in EDDI. The SPI and SSI showed similar behavior regarding  
 336 the trend in land cover type. A decrease in SPI and SSI is associated with an increase in the surface in  
 337 shrubland and grassland in “Centro,” forest in “Sur,” and barren land in “Norte Chico,” as well as a  
 338 decrease trend in savanna in “Norte Chico,” “Centro,” and “Sur.”

339 *4.3. Drought impacts on vegetation productivity within land cover*

340 *4.3.1. Vegetation productivity*

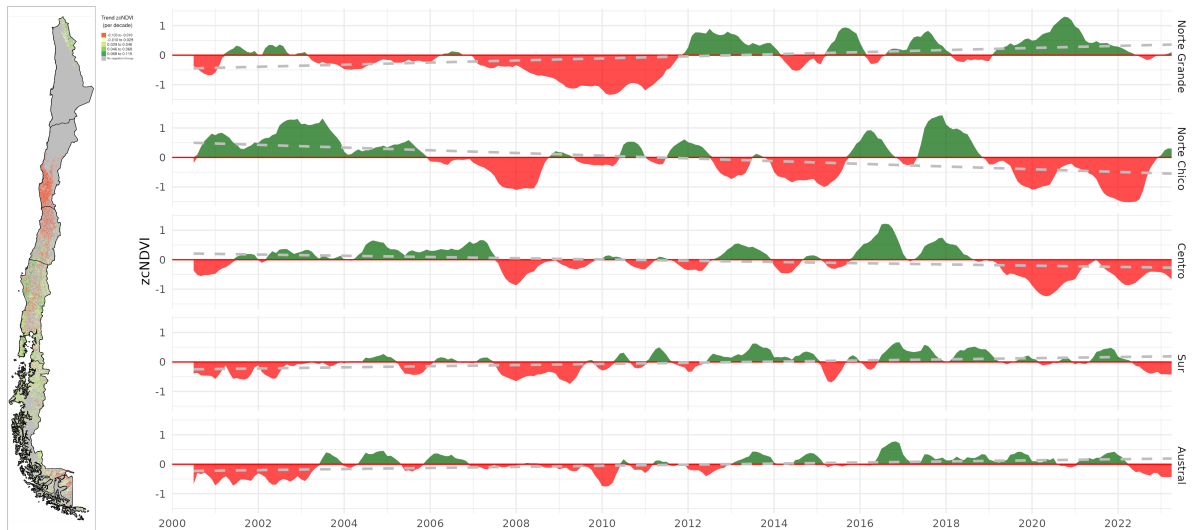


Figure 6: (a) Map of the linear trend of the index zcNDVI-6 for 2001–2023. Greener colors indicate a positive trend; red colors correspond to a negative trend and a decrease in vegetation productivity. Grey colors indicate either no vegetation or a change in land cover type for 2001–2022. (b) Temporal variation of zcNDVI-6 aggregated at macrozone level within continental Chile. Each horizontal panel corresponds to a macrozone from ‘Norte Grande’ to ‘Austral’.

341 In Figure 6 it is showed the spatial map of trends in zcNDVI (Figure 6a) and the temporal variation of  
 342 zcNDVI within the aggregated macrozones (Figure 6b). In “Norte Grande,” vegetation productivity, as per  
 343 the z-index, exhibits a yearly increase of 0.02 with respect to grassland and shrubland categories. There is  
 344 a negative trend in “Norte Chico” with -0.04 and “Centro” with -0.02 per decade. In the “Norte Chico,”  
 345 savanna (-0.05) has the lowest trend, and the rest of the types are around -0.04. In “Centro,” shrubland  
 346 reaches -0.06, grassland -0.05, and croplands and savanna -0.01 per decade. This could be associated either  
 347 with a reduction in vegetation surface, a decrease in biomass, or browning (Miranda et al., 2023). Vegetation  
 348 reached its lowest values since the year 2019, with an extreme condition in early 2020 and 2022 in the “Norte  
 349 Chico” and “Centro”. The “Sur” and “Austral” show a positive trend of around 0.016 per decade (Figure 6).  
 350 Despite the croplands suffering from drought just as badly as the native vegetation in “Norte Chico,” the  
 351 savanna and shrubland appears to be the region most affected by a negative trend in vegetation productivity.

352 *4.3.2. Correlation between vegetation productivity and drought indices*

353 Figure 7 is a map that shows the highest coefficient of determination ( $r^2$ , or rsq) found in the  
 354 regression analysis between different drought indicators and plant productivity over time. The spatial  
 355 variation of time scales reached per index is mostly for time scales above 12 months. In the case of SSI,  
 356 the predominant scales are 6 and 12 months. For all indices, to the north, the time scales are higher and  
 357 diminish toward the south until the south part of “Austral” increases. In Figure 8, the map of Pearson

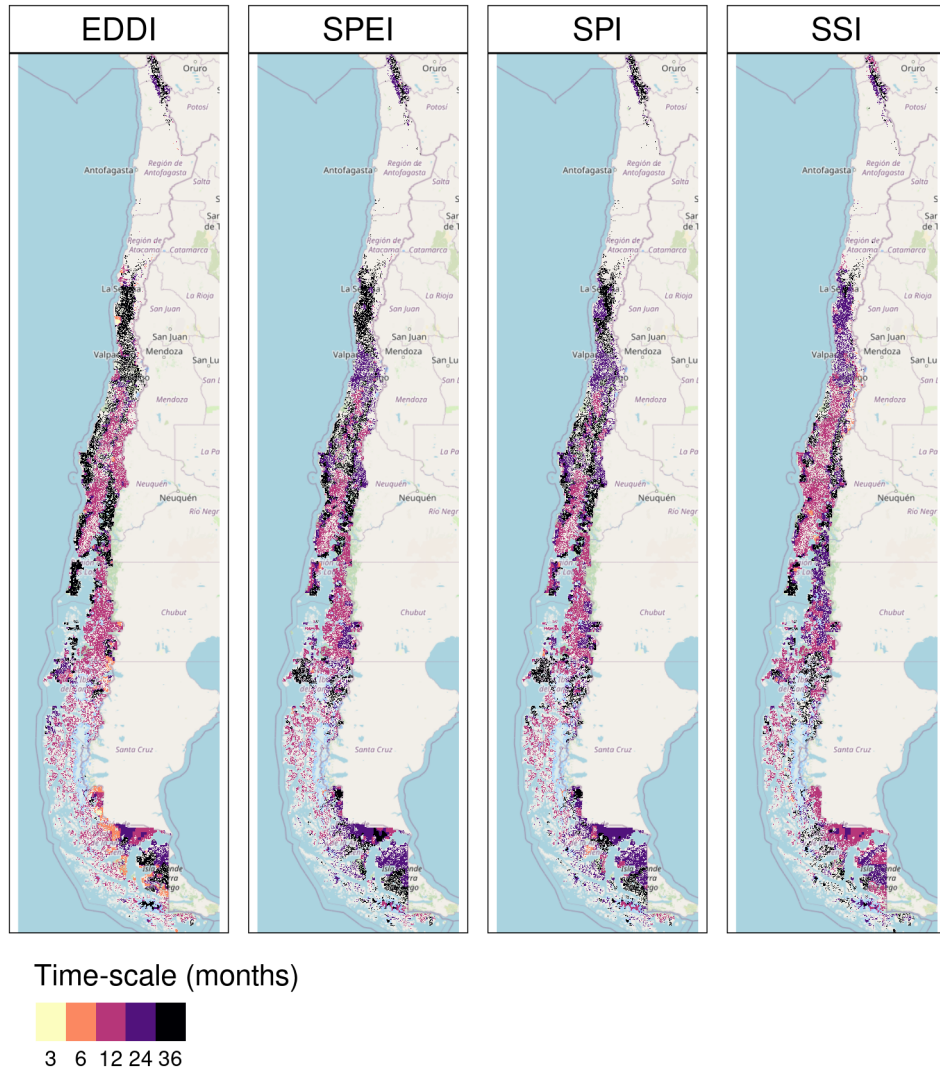


Figure 7: Time scales per drought index that reach the maximum coefficient of determination

correlation values is shown. The EDDI reached correlations above 0.5 between “Norte Chico” and “Sur.” The correlation changes from negative to positive toward the Andes Mountains and to the sea, just as in the northern part of “Austral.” The SPI and SPEI have similar results, with the higher values in “Norte Chico” and “Centro” being higher than 0.6. Following a similar spatial pattern as EDDI. The SSI showed to be the index that has a major spatial extension with a higher correlation. It has a similar correlation to SPI and SPEI for “Norte Chico” and “Sur,” but has improvements for “Sur.”

In Table 5, we aggregate per macrozone and landcover the correlation analysis presented in Figure 7 and Figure 8. According to what is shown, forests seem to be the most resistant to drought. Showing that only “Centro” is slightly ( $rsq = 0.25$ ) impacted by a 12-month soil moisture deficit (SSI-12). In the “Norte Chico” and to a lesser extent in the “Norte Grande,” it is evident that a SSI-12 with a  $rsq = 0.45$  and a decrease in water supply (SPI-36 and SPEI-24 with  $rsq = 0.28$  and 0.34, respectively) have an impact on grasslands. However, this type was unaffected by soil moisture, water supply, or demand in macrozones further south. The types that show to be most affected by variation in climate conditions are shrublands, savannas, and croplands. For savannas in “Norte Chico,” the SSI-12 and SPI-24 reached an  $rsq$  of 0.74

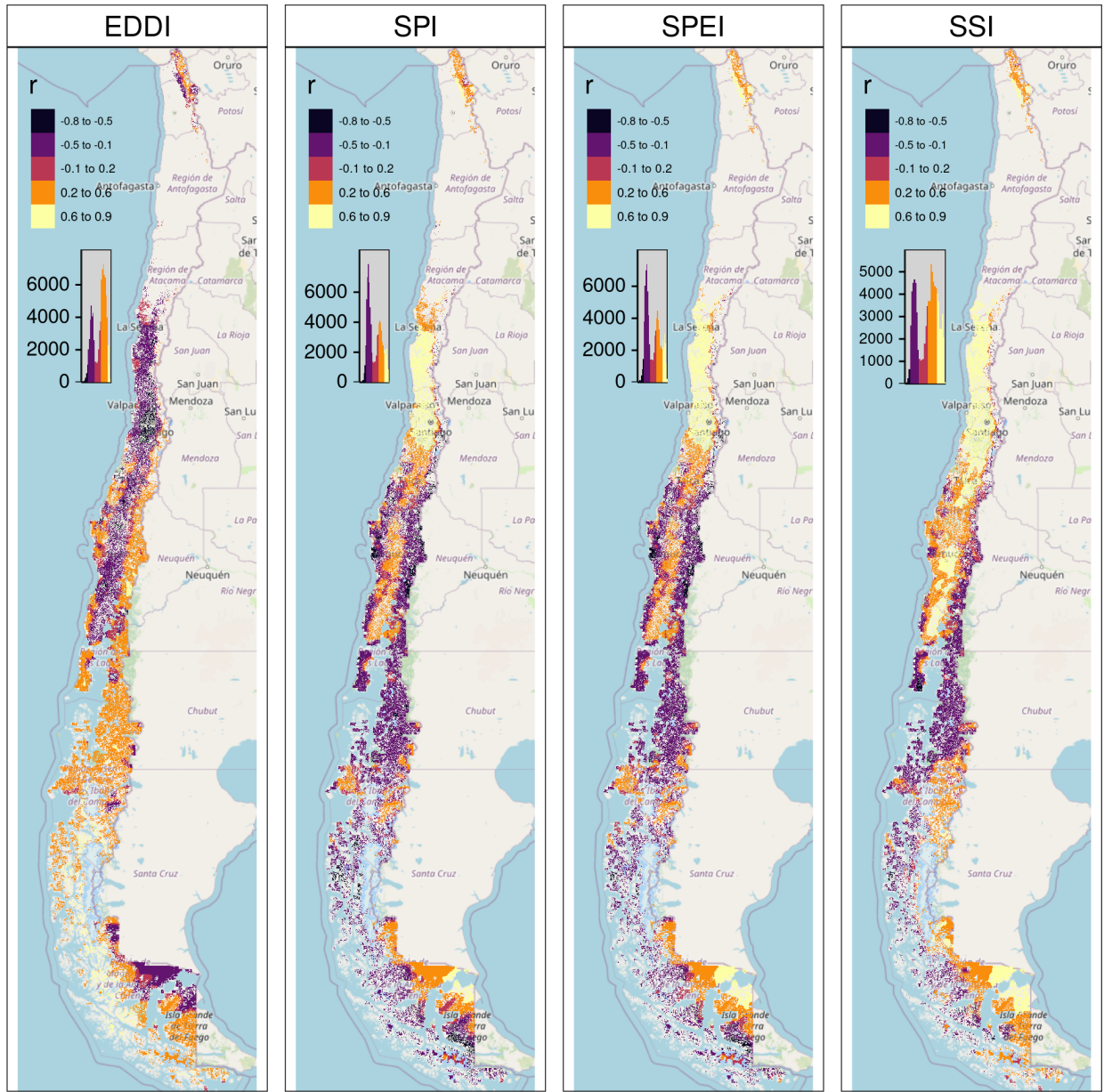


Figure 8: Pearson correlation value for the time scales and drought index that reach the maximum coefficient of determination

and 0.58, respectively. This value decreases to the south, but the SSI-12 is still the variable explaining more of the variation in vegetation productivity ( $rsq = 0.45$  in “Centro” and 0.2 in “Sur”). In the case of croplands, the SPEI-12, SPI-36, and SSI-12 explain between 45% and 66% of the variability in “Norte Chico.” The type of land most impacted by climatic variation was shrubland, where soil moisture explained 59% and precipitation, 37%, in “Norte Chico” and “Centro,” with SSI-12 being the most relevant variable, then SPI-36 in “Norte Chico” and SPI-24 in “Sur.”

Table 5: Summary per land cover macroclass and macrozone regarding the correlation between zcNDVI with the drought indices EDDI, SPI, SPEI, and SSI for time scales of 1, 3, 6, 12, 24, and 36. The numbers in each cell indicate the time scale that reached the maximum correlation for the land cover and macrozone, and the color indicates the strength of the r-squared obtained with the index and the time scale.

macrozone	Forest				Cropland				Grassland				Savanna				Shrubland			
	EDDI	SPI	SPEI	SSI	EDDI	SPI	SPEI	SSI	EDDI	SPI	SPEI	SSI	EDDI	SPI	SPEI	SSI	EDDI	SPI	SPEI	SSI
Norte Grande									36	36	36	12					36	12	36	12
Norte Chico					36	36	12	12	36	36	24	12	36	24	24	12	36	36	24	12
Centro	36	36	12	6	12	12	6	6	12	12	12	36	12	12	12	36	24	24	12	
Sur	36				6	6	6	6	6	6	6	12	6	6	6	6				
Austral	6	6									6	12	12	6	6	12	12	6	6	6
 r-squared																				

## 378 5. Discussion

### 379 5.1. Drought trend and attribution to land cover

380 Vicente-Serrano et al. (2022), in a study at the global scale of drought trends, indicate that there have not  
 381 been significant trends in meteorological drought since 1950. Also, state that the increase in hidrological  
 382 trend in some parts of the globe (northeast Brazil and the Mediterranean region) is related to changes  
 383 in land cover and specifically to the rapidly increasing irrigated area, which consequently increases water  
 384 extraction. Kogan et al. (2020) analyzed the agricultural drought impact globally and in the main grain  
 385 producer countries, finding that “since 1980, the Earth warming has not changed the drought area or  
 386 intensity.” In our study, we considered the variation in vegetation productivity in Chile for areas without  
 387 changes in land cover, to avoid misleading conclusions that could be related to the increase in water demand  
 388 due to land cover change. Our results show a contrasting perspective. There has been a significant trend  
 389 in the decline of vegetation productivity (zcNDVI) since 2000 for “Norte Chico” and “Centro,” which has  
 390 been extreme between 2020 and 2022, seemly due to an intense hydrological drought due to the persistance  
 391 of the mega drought (Garreaud et al., 2017). However, a rise in irrigated land doesn’t seem to have an  
 392 impact on this hydrological drought. Despite using the persistance mask for vegetation’s trend analysis,  
 393 cropland, which is the most water-demand type, showed a decrease trend in “Norte Chico” and “Centro.”  
 394 Also, there was an increase in barren land for both types. These changes are associated with a decrease  
 395 in water demand from vegetation. Nonetheless, we used the persistant land cover to ensure that the pixel  
 396 has the same class; in the case of croplands, it could happen that some areas had changed crops for others  
 397 with higher water consumption and consequently increase water demand. But this effect should be minor  
 398 compared to the results from land cover change at this scale of analysis.

399 On the other hand, for “Norte Chico” and “Centro,” our results show a decrease in trends of water supply  
 400 (SPI and SSI), which are higher at larger time scales, which is evidence of the hydrological drought. We say  
 401 that what happened in central Chile goes against what has been found on a global scale (Vicente-Serrano  
 402 et al., 2022; Kogan et al., 2020). This shows that the main cause of the hydrological drought in Chile was  
 403 a steady drop in water supply made worse by an increase in AED, but it seems that in zones most affected  
 404 by drought, the main cause is not an increase in water demand by vegetation like irrigated crops. Finally,  
 405 north-central Chile has experienced a decline in vegetation productivity across all macroclasses, which is  
 406 primarily attributable to variations in water supply and soil moisture. An increase in water demand, such  
 407 as an increase in the surface area of irrigated crops, could strengthen this trend.

408    5.2. Land cover types and their impact by drought

409    We discovered that croplands, savannas, and shrubland are the most susceptible to climatic changes and are  
410    most affected by the 12-month soil moisture deficit. In a study in the Yangtze River Basin in China, [Jiang et al. \(2020\)](#) analyzed the impact of drought on vegetation using the SPEI and the Enhanced Vegetation  
411    Index (EVI). They found that cropland was more sensitive to drought than grassland, showing that cropland  
412    responds strongly to short- and medium-term drought (< SPEI-6). In our case, the SPEI-12 was the one that  
413    most impacted the croplands in “Norte Chico” and “Centro.” In general, most studies show that croplands  
414    are most sensitive to short-term drought (< SPI-6) ([Zambrano et al., 2016](#); [Potopová et al., 2015](#); [Dai et al., 2020](#); [Rhee et al., 2010](#)). Short-term precipitation deficits impact soil water, and thus less water is available  
415    for plant growth. However, we found that in “Norte Chico,” an SPI-36 and SPEI-12 had a higher impact,  
416    which are associated with hydrological drought (long-term), and in “Centro,” an SPI-12 and SPEI-12. Thus,  
417    we attribute this impact to the hydrological drought that has decreased groundwater storage ([Taucare et al., 2024](#)), which in turn is impacted by long-term deficits, and consequently, the vegetation is more dependent on  
418    groundwater. In “Sur” and “Austral,” the correlations between drought indices and vegetation productivity  
419    decrease, as do the time scales that reach the maximum r-squared. What can be explained is that, south of  
420    “Centro,” predominate forest and grassland, the most resistant types. Also, drought episodes have been less  
421    frequent and intense. The drought episodes have had a lower impact on water availability for vegetation.

422    According to [Senf et al. \(2020\)](#), severe drought conditions in Europe are a significant cause of tree mortality.  
423    However, we found that forest is the type of land cover macroclass less affected by variation in drought indices,  
424    being the most resistant land cover class to drought. Supporting this is [Fathi-Taperasht et al. \(2022\)](#), who  
425    assert that Indian forests are the most drought-resistant and recover rapidly. Similarly, the work of [Wu et al. \(2024\)](#), who analyzed vegetation loss and recovery in response to meteorological drought in the humid  
426    subtropical Pearl River basin in China, indicates that forests showed higher drought resistance. Using  
427    Vegetation Optical Depth (VOD), kNDVI, and EVI, [Xiao et al. \(2023\)](#) test the resistance of ecosystems  
428    and find that ecosystems with more forests are better able to handle severe droughts than croplands. They  
429    attribute the difference to a deeper rooting depth of trees, a higher water storage capacity, and different  
430    water use strategies between forest and cropland ([Xiao et al., 2023](#)).

431    In contrast to what we obtained, [Venegas-González et al. \(2023\)](#), who studied *Cryptocarya alba* and  
432    *Beilschmiedia miersii* (both from the Lauraceae family) that live in sclerophyllous forests in Chile, found  
433    that the trees’ overall growth had slowed down. This could mean that the natural dynamics of their forests  
434    have changed. They attributed it to the cumulative effects of the unprecedented drought (i.e., hydrological  
435    drought). Thus, we attribute that forest to being the most resistant to drought, due to the fact that most  
436    of the species comprising it are highly resilient to water scarcity compared to the other land cover classes.  
437    Nonetheless, if we want to go deep in our analysis, we should use earth observation data that is able to  
438    capture a higher level of detail. For example, when we used MOD13A3 with a 1km spatial resolution to  
439    measure vegetation condition, it took the average condition of 1 square kilometer. Then, to use remote  
440    sensing to look at how a certain type of forest (like sclerophyllous forest) changes in response to drought on  
441    a local level, we should use operational products with higher spatial resolutions, like those from Landsat or  
442    Sentinel. This will let us do a more thorough analysis.

443    5.3. Soil moisture, vegetation productivity, and agricultural drought.

444    The main external factors that affect biomass production by vegetation are actual evapotranspiration and  
445    soil moisture, and the rate of ET in turn depends on the availability of water storage in the root zone.  
446    Thus, soil moisture plays a key role in land carbon uptake and, consequently, in the production of biomass  
447    ([Humphrey et al., 2021](#)). Moreover, [Zhang et al. \(2022\)](#) indicate there is a bidirectional causality between  
448    soil moisture and vegetation productivity. Lastly, some studies have redefined agricultural drought as soil  
449    moisture drought from a hydrological perspective ([Van Loon et al., 2016](#); [Samaniego et al., 2018](#)). Even  
450    though soil moisture is the external factor most determinant of vegetation biomass, there are multiple internal  
451    factors, such as species, physiological characteristics, and plant hydraulics, that would affect vegetation

456 productivity. Because of that, we believe that agricultural drought, referring to the drought that impacts  
457 vegetation productivity, is the most proper term, as originally defined by [Wilhite and Glantz \(1985\)](#).

458 The study results showed that the soil moisture-based drought index (SSI) was better at explaining vegeta-  
459 tion productivity across land cover macroclasses than meteorological drought indices like SPI, SPEI, and  
460 EDDI. In the early growing season and especially in irrigated rather than rainfed croplands, soil moisture  
461 has better skills than SPI and SPEI for estimating gross primary production (GPP). This according to  
462 [Chatterjee et al. \(2022\)](#) evaluation of the SPI and SPEI and their correlation with GPP in the CONUS.  
463 Also, [Zhou et al. \(2021\)](#) indicate that the monthly scaled Standardized Water Deficit Index (SWDI) can  
464 accurately show the effects of agricultural drought in most of China. [Nicolai-Shaw et al. \(2017\)](#) also looked  
465 at the time-lag between the SWDI and the Vegetation Condition Index (VCI). They found that there was  
466 little to no time-lag in croplands but a greater time-lag in forests.

467 In our case, there is strong spatial variability throughout Chile and between classes, mainly attributable to  
468 climate heterogeneity, hydrological status, or vegetation resistance to water scarcity. The semi-arid “Norte  
469 Chico” and the Mediterranean “Centro” were where SSI had the best performance. In Chile, medium-term  
470 deficits of 12 months are more relevant in the response of vegetation, which decreases to the south, and in the  
471 case of croplands, they seem to react in a shorter time, with six months (SSI-6) in “Centro.” This variation  
472 for croplands could be related to the fact that in “Norte Chico,” the majority of crops are irrigated, but  
473 to the south there is a higher proportion of rainfed agriculture, which is most dependent on the short-term  
474 availability of water. Rather, in the “Norte Chico,” the orchards are more dependent on the storage of water  
475 in dams of groundwater reservoirs, which are affected by long-term drought (e.g., SPI-36).

#### 476 5.4. Future outlook (to complete)

## 477 6. Conclusion

478 There is a trend toward decreasing water supply in most parts of Chile, particularly in the “Centro” and  
479 “Norte Chico” regions. The whole country showed an increase in AED. Vegetation productivity only showed  
480 a decrease in the “Norte Chico” and “Centro,” being highest for shrubland and croplands. Forest is the land  
481 cover most resistant to drought, as shown along Chile, and shrubland and cropland are the most sensitive.

482 A soil moisture deficit of 12 months (SSI-12) is highly correlated with vegetation productivity for the land  
483 cover classes of shrubland, savannas, croplands, and forest in “Norte Chico” and “Centro.” For the southern  
484 part of the country with humid conditions, the correlation with SSI decreases. Soil moisture overcomes  
485 the capacity to explain vegetation productivity over the supply and demand drought indices in the entire  
486 territory.

487 The variation in vegetation productivity appears to be associated with climate variation rather than an-  
488 thropogenic factors (e.g., an increase in water demand by irrigated crops). Even though switching to more  
489 demanding crops on the land could increase the impact of drought on vegetation, this would need to be  
490 more thoroughly investigated, for instance at the watershed level.

491 The results of this study could help in the development of a robust forecasting system for land cover classes  
492 in Chile, helping to improve preparedness for climate change impacts on vegetation.

## 493 Supplementary material

## 494 References

- 495 Abramowitz, M., Stegun, I.A., 1968. Handbook of mathematical functions with formulas, graphs, and mathematical tables.  
496 volume 55. US Government printing office.

- 497 Aceituno, P., Boisier, J.P., Garreaud, R., Rondanelli, R., Rutllant, J.A., 2021. Climate and Weather in Chile, in: Fernández,  
 498 B., Gironás, J. (Eds.), Water Resources of Chile. Springer International Publishing, Cham. volume 8, pp. 7–29. URL:  
 499 [http://link.springer.com/10.1007/978-3-030-56901-3\\_2](http://link.springer.com/10.1007/978-3-030-56901-3_2).
- 500 AghaKouchak, A., 2014. A baseline probabilistic drought forecasting framework using standardized soil moisture index: application to the 2012 United States drought. *Hydrology and Earth System Sciences* 18, 2485–2492. URL:  
 501 <https://hess.copernicus.org/articles/18/2485/2014/>, doi:10.5194/hess-18-2485-2014.
- 502 AghaKouchak, A., Mirchi, A., Madani, K., Di Baldassarre, G., Nazemi, A., Alborzi, A., Anjileli, H., Azarderakhsh, M., Chiang,  
 503 F., Hassanzadeh, E., Huning, L.S., Mallakpour, I., Martinez, A., Mazdiyasni, O., Moftakhari, H., Norouzi, H., Sadegh,  
 504 M., Sadeqi, D., Van Loon, A.F., Wanders, N., 2021. Anthropogenic Drought: Definition, Challenges, and Opportunities.  
 505 *Reviews of Geophysics* 59, e2019RG000683. URL: <https://agupubs.onlinelibrary.wiley.com/doi/10.1029/2019RG000683>,  
 506 doi:10.1029/2019RG000683.
- 507 Akinyemi, F.O., 2021. Vegetation Trends, Drought Severity and Land Use-Land Cover Change during the Growing Season in  
 508 Semi-Arid Contexts. *Remote Sensing* 2021, Vol. 13, Page 836 13, 836. URL: <https://www.mdpi.com/2072-4292/13/5/836/htm>, doi:10.3390/RS13050836. publisher: Multidisciplinary Digital Publishing Institute.
- 509 Bakker, K., 2012. Water Security: Research Challenges and Opportunities. *Science* 337, 914–915. URL: <https://www.science.org/doi/10.1126/science.1226337>, doi:10.1126/science.1226337.
- 510 Beck, H.E., McVicar, T.R., Vergopolan, N., Berg, A., Lutsko, N.J., Dufour, A., Zeng, Z., Jiang, X., van Dijk, A.I.J.M., Miralles,  
 511 D.G., 2023. High-resolution (1 km) Köppen-Geiger maps for 1901–2099 based on constrained CMIP6 projections. *Scientific  
 512 Data* 10. URL: <http://dx.doi.org/10.1038/s41597-023-02549-6>, doi:10.1038/s41597-023-02549-6.
- 513 Beguería, S., Vicente-Serrano, S.M., 2023. SPEI: Calculation of the Standardized Precipitation-Evapotranspiration Index.  
 514 URL: <https://CRAN.R-project.org/package=SPEI>.
- 515 Boisier, J.P., Alvarez-Garreton, C., Cordero, R.R., Damiani, A., Gallardo, L., Garreaud, R.D., Lambert, F., Ramallo, C.,  
 516 Rojas, M., Rondanelli, R., 2018. Anthropogenic drying in central-southern Chile evidenced by long-term observations  
 517 and climate model simulations. *Elementa* 6, 74. URL: <https://www.elementascience.org/article/10.1525/elementa.328/>,  
 518 doi:10.1525/elementa.328.
- 519 Calvin, K., Dasgupta, D., Krinner, G., Mukherji, A., Thorne, P.W., Trisos, C., Romero, J., Aldunce, P., Barrett, K., Blanco,  
 520 G., Cheung, W.W., Connors, S., Denton, F., Diongue-Niang, A., Dodman, D., Garschagen, M., Geden, O., Hayward, B.,  
 521 Jones, C., Jotzo, F., Krug, T., Lasco, R., Lee, Y.Y., Masson-Delmotte, V., Meinshausen, M., Mintenbeck, K., Mokssit, A.,  
 522 Otto, F.E., Pathak, M., Pirani, A., Poloczanska, E., Pörtner, H.O., Revi, A., Roberts, D.C., Roy, J., Ruane, A.C., Skea,  
 523 J., Shukla, P.R., Slade, R., Slangen, A., Sokona, Y., Sörensson, A.A., Tignor, M., Van Vuuren, D., Wei, Y.M., Winkler,  
 524 H., Zhai, P., Zommers, Z., Hourcade, J.C., Johnson, F.X., Pachauri, S., Simpson, N.P., Singh, C., Thomas, A., Totin, E.,  
 525 Arias, P., Bustamante, M., Elgizouli, I., Flato, G., Howden, M., Méndez-Vallejo, C., Pereira, J.J., Pichs-Madruga, R., Rose,  
 526 S.K., Saheb, Y., Sánchez Rodríguez, R., Ürge Vorsatz, D., Xiao, C., Yassa, N., Alegría, A., Armour, K., Bednar-Friedl, B.,  
 527 Blok, K., Cissé, G., Dentener, F., Eriksen, S., Fischer, E., Garner, G., Guiavarch, C., Haasnoot, M., Hansen, G., Hauser, M.,  
 528 Hawkins, E., Hermans, T., Kopp, R., Leprince-Ringuet, N., Lewis, J., Ley, D., Ludden, C., Niamir, L., Nicholls, Z., Some,  
 529 S., Szopa, S., Trewn, B., Van Der Wijst, K.I., Winter, G., Witting, M., Birt, A., Ha, M., Romero, J., Kim, J., Haites, E.F.,  
 530 Jung, Y., Stavins, R., Birt, A., Ha, M., Orendain, D.J.A., Ignon, L., Park, S., Park, Y., Reisinger, A., Cammaramo, D.,  
 531 Fischlin, A., Fuglestvedt, J.S., Hansen, G., Ludden, C., Masson-Delmotte, V., Matthews, J.R., Mintenbeck, K., Pirani, A.,  
 532 Poloczanska, E., Leprince-Ringuet, N., Péan, C., 2023. IPCC, 2023: Climate Change 2023: Synthesis Report. Contribution  
 533 of Working Groups I, II and III to the Sixth Assessment Report of the Intergovernmental Panel on Climate Change [Core  
 534 Writing Team, H. Lee and J. Romero (eds.)]. IPCC, Geneva, Switzerland. Technical Report. Intergovernmental Panel on  
 535 Climate Change (IPCC). URL: <https://www.ipcc.ch/report/ar6/syr/>.
- 536 Chamlng, M., Bera, B., 2020. Spatio-temporal Patterns of Land Use/Land Cover Change in the Bhutan–Bengal Foothill Region  
 537 Between 1987 and 2019: Study Towards Geospatial Applications and Policy Making. *Earth Systems and Environment* 4,  
 538 117–130. URL: <http://link.springer.com/10.1007/s41748-020-00150-0>, doi:10.1007/s41748-020-00150-0.
- 539 Chatterjee, S., Desai, A.R., Zhu, J., Townsend, P.A., Huang, J., 2022. Soil moisture as an essential component for delineating  
 540 and forecasting agricultural rather than meteorological drought. *Remote Sensing of Environment* 269, 112833. URL:  
 541 <https://linkinghub.elsevier.com/retrieve/pii/S0034425721005538>, doi:10.1016/j.rse.2021.112833.
- 542 Chen, J., Shao, Z., Huang, X., Zhuang, Q., Dang, C., Cai, B., Zheng, X., Ding, Q., 2022. Assessing the impact of drought-  
 543 land cover change on global vegetation greenness and productivity. *Science of The Total Environment* 852, 158499. URL:  
 544 <https://linkinghub.elsevier.com/retrieve/pii/S004896972205598X>, doi:10.1016/j.scitotenv.2022.158499.
- 545 Crausbay, S.D., Ramirez, A.R., Carter, S.L., Cross, M.S., Hall, K.R., Bathke, D.J., Betancourt, J.L., Colt, S., Cravens, A.E.,  
 546 Dalton, M.S., Dunham, J.B., Hay, L.E., Hayes, M.J., McEvoy, J., McNutt, C.A., Moritz, M.A., Nislow, K.H., Raheem, N.,  
 547 Sanford, T., 2017. Defining Ecological Drought for the Twenty-First Century. *Bulletin of the American Meteorological Society*  
 548 98, 2543–2550. URL: <https://journals.ametsoc.org/view/journals/bams/98/12/bams-d-16-0292.1.xml>, doi:10.1175/BAMS-D-  
 549 16-0292.1. publisher: American Meteorological Society.
- 550 Dai, M., Huang, S., Huang, Q., Leng, G., Guo, Y., Wang, L., Fang, W., Li, P., Zheng, X., 2020. Assessing agricultural drought  
 551 risk and its dynamic evolution characteristics. *Agricultural Water Management* 231, 106003. URL: <https://linkinghub.elsevier.com/retrieve/pii/S0378377419316531>, doi:10.1016/j.agwat.2020.106003.
- 552 Didan, K., 2015. MOD13Q1 MODIS/Terra Vegetation Indices 16-Day L3 Global 250m SIN Grid V006. Technical Report.  
 553 NASA EOSDIS Land Processes DAAC. doi:<http://dx.doi.org/10.5067/MODIS/MOD13Q1.006>.
- 554 Farahmand, A., AghaKouchak, A., 2015. A generalized framework for deriving nonparametric standardized drought indicators.  
 555 *Advances in Water Resources* 76, 140–145. URL: <https://linkinghub.elsevier.com/retrieve/pii/S0309170814002322>, doi:10.  
 556 1016/j.advwatres.2014.11.012.
- 557 Fathi-Taperasht, A., Shafizadeh-Moghadam, H., Minaei, M., Xu, T., 2022. Influence of drought duration and severity on

- 562 drought recovery period for different land cover types: evaluation using MODIS-based indices. Ecological Indicators 141,  
 563 109146. URL: <https://linkinghub.elsevier.com/retrieve/pii/S1470160X22006185>, doi:[10.1016/j.ecolind.2022.109146](https://doi.org/10.1016/j.ecolind.2022.109146).
- 564 Ford, T.W., Otkin, J.A., Quiring, S.M., Lisonbee, J., Woloszyn, M., Wang, J., Zhong, Y., 2023. Flash Drought Indicator  
 565 Intercomparison in the United States. Journal of Applied Meteorology and Climatology 62, 1713–1730. URL: <https://journals.ametsoc.org/view/journals/apme/62/12/JAMC-D-23-0081.1.xml>, doi:[10.1175/JAMC-D-23-0081.1](https://doi.org/10.1175/JAMC-D-23-0081.1).
- 566 Fuentes, I., Fuster, R., Avilés, D., Vervoort, W., 2021. Water scarcity in central Chile: the effect of climate and land cover  
 567 changes on hydrologic resources. Hydrological Sciences Journal 66, 1028–1044. URL: <https://www.tandfonline.com/doi/full/10.1080/02626667.2021.1903475>, doi:[10.1080/02626667.2021.1903475](https://doi.org/10.1080/02626667.2021.1903475).
- 568 Garreaud, R., Alvarez-Garreton, C., Barichivich, J., Boisier, J.P., Christie, D., Galleguillos, M., LeQuesne, C., McPhee,  
 569 J., Zambrano-Bigiarini, M., 2017. The 2010–2015 mega drought in Central Chile: Impacts on regional hydroclimate and  
 570 vegetation. Hydrology and Earth System Sciences Discussions 2017, 1–37. URL: <http://www.hydrol-earth-syst-sci-discuss.net/hess-2017-191/>, doi:[10.5194/hess-2017-191](https://doi.org/10.5194/hess-2017-191).
- 571 Garreaud, R.D., 2009. The Andes climate and weather. Advances in Geosciences 22, 3–11. URL: <https://adgeo.copernicus.org/articles/22/3/2009/>, doi:[10.5194/adgeo-22-3-2009](https://doi.org/10.5194/adgeo-22-3-2009).
- 572 Gebrechorkos, S.H., Peng, J., Dyer, E., Miralles, D.G., Vicente-Serrano, S.M., Funk, C., Beck, H.E., Asfaw, D.T., Singer, M.B.,  
 573 Dadson, S.J., 2023. Global high-resolution drought indices for 1981–2022. Earth System Science Data 15, 5449–5466. URL:  
 574 <https://essd.copernicus.org/articles/15/5449/2023/>, doi:[10.5194/essd-15-5449-2023](https://doi.org/10.5194/essd-15-5449-2023).
- 575 Hao, Z., AghaKouchak, A., 2013. Multivariate Standardized Drought Index: A parametric multi-index model. Advances in Water  
 576 Resources 57, 12–18. URL: <https://linkinghub.elsevier.com/retrieve/pii/S0309170813000493>, doi:[10.1016/j.advwatres.2013.03.009](https://doi.org/10.1016/j.advwatres.2013.03.009).
- 577 Hargreaves, G.H., 1994. Defining and Using Reference Evapotranspiration. Journal of Irrigation and Drainage Engineering 120,  
 578 1132–1139. URL: <https://ascelibrary.org/doi/10.1061/%28ASCE%290733-9437%281994%29120%3A6%281132%29>, doi:[10.1061/\(ASCE\)0733-9437\(1994\)120:6\(1132\)](https://doi.org/10.1061/(ASCE)0733-9437(1994)120:6(1132)).
- 579 Hargreaves, G.H., Samani, Z.A., 1985. Reference crop evapotranspiration from temperature. Applied engineering in agriculture  
 580 1, 96–99.
- 581 Heim, R.R., 2002. A Review of Twentieth-Century Drought Indices Used in the United States. Bulletin of the American  
 582 Meteorological Society 83, 1149–1166. URL: <https://journals.ametsoc.org/doi/10.1175/1520-0477-83.8.1149>, doi:[10.1175/1520-0477-83.8.1149](https://doi.org/10.1175/1520-0477-83.8.1149).
- 583 Hijmans, R.J., 2023. terra: Spatial Data Analysis. URL: <https://CRAN.R-project.org/package=terra>.
- 584 Ho, T.K., 1995. Random decision forests, in: Proceedings of 3rd international conference on document analysis and recognition,  
 585 IEEE. pp. 278–282.
- 586 Hobbins, M.T., Wood, A., McEvoy, D.J., Huntington, J.L., Morton, C., Anderson, M., Hain, C., 2016. The Evaporative Demand  
 587 Drought Index. Part I: Linking Drought Evolution to Variations in Evaporative Demand. Journal of Hydrometeorology 17,  
 588 1745–1761. URL: <https://journals.ametsoc.org/doi/10.1175/JHM-D-15-0121.1>, doi:[10.1175/JHM-D-15-0121.1](https://doi.org/10.1175/JHM-D-15-0121.1).
- 589 Homer, C., Dewitz, J., Jin, S., Xian, G., Costello, C., Danielson, P., Gass, L., Funk, M., Wickham, J., Stelman, S., Auch, R.,  
 590 Riitters, K., 2020. Conterminous United States land cover change patterns 2001–2016 from the 2016 National Land Cover  
 591 Database. ISPRS Journal of Photogrammetry and Remote Sensing 162, 184–199. URL: <https://linkinghub.elsevier.com/retrieve/pii/S0924271620300587>, doi:[10.1016/j.isprsjprs.2020.02.019](https://doi.org/10.1016/j.isprsjprs.2020.02.019).
- 592 Hufkens, K., Stauffer, R., Campitelli, E., 2019. The ecwmfr package: an interface to ECMWF API endpoints. URL: <https://bluegreen-labs.github.io/ecwmfr/>.
- 593 Humphrey, V., Berg, A., Ciais, P., Gentine, P., Jung, M., Reichstein, M., Seneviratne, S.I., Frankenberg, C., 2021. Soil  
 594 moisture–atmosphere feedback dominates land carbon uptake variability. Nature 592, 65–69. URL: <https://www.nature.com/articles/s41586-021-03325-5>, doi:[10.1038/s41586-021-03325-5](https://doi.org/10.1038/s41586-021-03325-5).
- 595 IPCC, 2013. Climate Change 2013: The Physical Science Basis. Contribution of Working Group I to the Fifth Assessment  
 596 Report of the Intergovernmental Panel on Climate Change. Cambridge University Press, Cambridge, UK; New York, USA.  
 597 URL: [www.climatechange2013.org](http://www.climatechange2013.org), doi:[10.1017/CBO9781107415324](https://doi.org/10.1017/CBO9781107415324).
- 598 Jiang, W., Wang, L., Feng, L., Zhang, M., Yao, R., 2020. Drought characteristics and its impact on changes in surface  
 599 vegetation from 1981 to 2015 in the Yangtze River Basin, China. International Journal of Climatology 40, 3380–3397. URL:  
 600 <https://rmets.onlinelibrary.wiley.com/doi/10.1002/joc.6403>, doi:[10.1002/joc.6403](https://doi.org/10.1002/joc.6403).
- 601 Kendall, M., 1975. Rank correlation methods (4th ed. 2d impression). Griffin.
- 602 Kogan, F., Guo, W., Yang, W., 2020. Near 40-year drought trend during 1981–2019 earth warming and food security. Geomatics,  
 603 Natural Hazards and Risk 11, 469–490. URL: <https://www.tandfonline.com/doi/full/10.1080/19475705.2020.1730452>, doi:[10.1080/19475705.2020.1730452](https://doi.org/10.1080/19475705.2020.1730452).
- 604 Kuhn, M., Wickham, H., 2020. Tidymodels: a collection of packages for modeling and machine learning using tidyverse  
 605 principles. URL: <https://www.tidymodels.org>.
- 606 Laimighofer, J., Laaha, G., 2022. How standard are standardized drought indices? Uncertainty components for the SPI  
 607 & SPEI case. Journal of Hydrology 613, 128385. URL: <https://linkinghub.elsevier.com/retrieve/pii/S0022169422009544>, doi:[10.1016/j.jhydrol.2022.128385](https://doi.org/10.1016/j.jhydrol.2022.128385).
- 608 Li, H., Choy, S., Zaminpardaz, S., Wang, X., Liang, H., Zhang, K., 2024. Flash drought monitoring using diurnal-provided  
 609 evaporative demand drought index. Journal of Hydrology 633, 130961. URL: <https://linkinghub.elsevier.com/retrieve/pii/S002216942400355X>, doi:[10.1016/j.jhydrol.2024.130961](https://doi.org/10.1016/j.jhydrol.2024.130961).
- 610 Li, W., Migliavacca, M., Forkel, M., Denissen, J.M.C., Reichstein, M., Yang, H., Duveiller, G., Weber, U., Orth, R., 2022.  
 611 Widespread increasing vegetation sensitivity to soil moisture. Nature Communications 13, 3959. URL: <https://www.nature.com/articles/s41467-022-31667-9>, doi:[10.1038/s41467-022-31667-9](https://doi.org/10.1038/s41467-022-31667-9).
- 612 Liu, X., Yu, S., Yang, Z., Dong, J., Peng, J., 2024. The first global multi-timescale daily SPEI dataset from 1982 to 2021.

- 627 Scientific Data 11, 223. URL: <https://www.nature.com/articles/s41597-024-03047-z>, doi:10.1038/s41597-024-03047-z.
- 628 Luebert, F., Pliscott, P., 2022. The vegetation of Chile and the EcoVeg approach in the context of the International Vegetation  
629 Classification project. *Vegetation Classification and Survey* 3, 15–28. URL: <https://vcs.pensoft.net/article/67893/>, doi:10.  
630 3897/VCS.67893.
- 631 Luo, L., Apps, D., Arcand, S., Xu, H., Pan, M., Hoerling, M., 2017. Contribution of temperature and precipitation anomalies to  
632 the California drought during 2012–2015. *Geophysical Research Letters* 44, 3184–3192. URL: <https://agupubs.onlinelibrary.wiley.com/doi/10.1002/2016GL072027>, doi:10.1002/2016GL072027.
- 633 Luyssaert, S., Jammet, M., Stoy, P.C., Estel, S., Pongratz, J., Ceschia, E., Churkina, G., Don, A., Erb, K., Ferlicoq, M.,  
634 Gielen, B., Grünwald, T., Houghton, R.A., Klumpp, K., Knohl, A., Kolb, T., Kuemmerle, T., Laurila, T., Lohila, A.,  
635 Loustau, D., McGrath, M.J., Meyfroidt, P., Moors, E.J., Naudts, K., Novick, K., Otto, J., Pilegaard, K., Pio, C.A., Rambal,  
636 S., Rebmann, C., Ryder, J., Suyker, A.E., Varlagin, A., Wattenbach, M., Dolman, A.J., 2014. Land management and  
637 land-cover change have impacts of similar magnitude on surface temperature. *Nature Climate Change* 4, 389–393. URL:  
638 <https://www.nature.com/articles/nclimate2196>, doi:10.1038/nclimate2196.
- 639 Masson-Delmotte, V., P.Z.A.P.S.L.C.C.P.S.B.N.C.Y.C.L.G.M.I.G.M.H.K.L.E.L.J.B.R.M.T.K.M.T.W.O.Y.R.Y.a.B.Z.e., 2021.  
640 IPCC, 2021: Climate Change 2021: The Physical Science Basis. Contribution of Working Group I to the Sixth Assessment  
641 Report of the Intergovernmental Panel on Climate Change. Technical Report. URL: <https://www.ipcc.ch/>. publication  
642 Title: Cambridge University Press. In Press.
- 643 McEvoy, D.J., Huntington, J.L., Hobbins, M.T., Wood, A., Morton, C., Anderson, M., Hain, C., 2016. The Evaporative Demand  
644 Drought Index. Part II: CONUS-Wide Assessment against Common Drought Indicators. *Journal of Hydrometeorology* 17,  
645 1763–1779. URL: <http://journals.ametsoc.org/doi/10.1175/JHM-D-15-0122.1>, doi:10.1175/JHM-D-15-0122.1.
- 646 Meroni, M., Rembold, F., Fasbender, D., Vrieling, A., 2017. Evaluation of the Standardized Precipitation Index as an early  
647 predictor of seasonal vegetation production anomalies in the Sahel. *Remote Sensing Letters* 8, 301–310. URL: <http://www.tandfonline.com/doi/abs/10.1080/2150704X.2016.1264020>.
- 648 Miranda, A., Lara, A., Altamirano, A., Di Bella, C., González, M.E., Julio Camarero, J., 2020. Forest browning trends in  
649 response to drought in a highly threatened mediterranean landscape of South America. *Ecological Indicators* 115, 106401.  
650 URL: <https://linkinghub.elsevier.com/retrieve/pii/S1470160X20303381>, doi:10.1016/j.ecolind.2020.106401.
- 651 Miranda, A., Syphard, A.D., Berdugo, M., Carrasco, J., Gómez-González, S., Ovalle, J.F., Delpiano, C.A., Vargas, S.,  
652 Squeo, F.A., Miranda, M.D., Dobbs, C., Mentler, R., Lara, A., Garreaud, R., 2023. Widespread synchronous decline  
653 of Mediterranean-type forest driven by accelerated aridity. *Nature Plants* 9, 1810–1817. URL: <https://www.nature.com/articles/s41477-023-01541-7>, doi:10.1038/s41477-023-01541-7.
- 654 Muñoz-Sabater, J., Dutra, E., Agustí-Panareda, A., Albergel, C., Arduini, G., Balsamo, G., Boussetta, S., Choulga, M.,  
655 Harrigan, S., Hersbach, H., Martens, B., Miralles, D.G., Piles, M., Rodríguez-Fernández, N.J., Zsoter, E., Buontempo, C.,  
656 Thépaut, J.N., 2021. ERA5-Land: a state-of-the-art global reanalysis dataset for land applications. *Earth System Science  
657 Data* 13, 4349–4383. URL: <https://essd.copernicus.org/articles/13/4349/2021/>, doi:10.5194/essd-13-4349-2021.
- 658 Narasimhan, B., Srinivasan, R., 2005. Development and evaluation of Soil Moisture Deficit Index (SMDI) and Evapotranspi-  
659 ration Deficit Index (ETDI) for agricultural drought monitoring. *Agricultural and Forest Meteorology* 133, 69–88. URL:  
660 <https://linkinghub.elsevier.com/retrieve/pii/S0168192305001565>, doi:10.1016/j.agrformet.2005.07.012.
- 661 Nicolai-Shaw, N., Zscheischler, J., Hirschi, M., Gudmundsson, L., Seneviratne, S.I., 2017. A drought event composite analysis  
662 using satellite remote-sensing based soil moisture. *Remote Sensing of Environment* 203, 216–225. URL: [https://linkinghub.elsevier.com/retrieve/pii/S0034425717302729](https://linkinghub.<br/>663 elsevier.com/retrieve/pii/S0034425717302729), doi:10.1016/j.rse.2017.06.014.
- 664 Noguera, I., Vicente-Serrano, S.M., Domínguez-Castro, F., 2022. The Rise of Atmospheric Evaporative Demand Is Increasing  
665 Flash Droughts in Spain During the Warm Season. *Geophysical Research Letters* 49, e2021GL097703. URL: [https://agupubs.onlinelibrary.wiley.com/doi/10.1029/2021GL097703](https://<br/>666 agupubs.onlinelibrary.wiley.com/doi/10.1029/2021GL097703), doi:10.1029/2021GL097703.
- 667 Pebesma, E., 2018. Simple Features for R: Standardized Support for Spatial Vector Data. *The R Journal* 10, 439–446. URL:  
668 <https://doi.org/10.32614/RJ-2018-009>, doi:10.32614/RJ-2018-009.
- 669 Pebesma, E., Bivand, R., 2023. Spatial Data Science: With applications in R. Chapman and Hall/CRC, London. URL:  
670 <https://r-spatial.org/book/>.
- 671 Peng, D., Zhang, B., Wu, C., Huete, A.R., Gonsamo, A., Lei, L., Ponce-Campos, G.E., Liu, X., Wu, Y., 2017. Country-level  
672 net primary production distribution and response to drought and land cover change. *Science of The Total Environment* 574,  
673 65–77. URL: <https://linkinghub.elsevier.com/retrieve/pii/S0048969716319507>, doi:10.1016/j.scitotenv.2016.09.033.
- 674 Pitman, A.J., De Noblet-Ducoudré, N., Avila, F.B., Alexander, L.V., Boisier, J.P., Brovkin, V., Delire, C., Cruz, F., Donat,  
675 M.G., Gayler, V., Van Den Hurk, B., Reick, C., Volodko, A., 2012. Effects of land cover change on temperature and  
676 rainfall extremes in multi-model ensemble simulations. *Earth System Dynamics* 3, 213–231. URL: [https://esd.copernicus.org/articles/3/213/2012/](https://esd.copernicus.org/<br/>677 articles/3/213/2012/), doi:10.5194/esd-3-213-2012.
- 678 Potopová, V., Stepánek, P., Mozný, M., Türkott, L., Soukup, J., 2015. Performance of the standarised precipitation evapotran-  
679 spiration index at various lags for agricultural drought risk assessment in the {C}zech {R}epublic. *Agricultural and Forest  
680 Meteorology* 202, 26–38.
- 681 R Core Team, 2023. R: A Language and Environment for Statistical Computing. R Foundation for Statistical Computing,  
682 Vienna, Austria. URL: <https://www.R-project.org/>.
- 683 Rhee, J., Im, J., Carbone, G.J., 2010. Monitoring agricultural drought for arid and humid regions using multi-sensor remote  
684 sensing data. *Remote Sensing of Environment* 114, 2875–2887. URL: [http://www.sciencedirect.com/science/article/pii/S003442571000221X](http://www.sciencedirect.com/science/article/pii/<br/>685 S003442571000221X), doi:10.1016/j.rse.2010.07.005.
- 686 Samaniego, L., Thober, S., Kumar, R., Wanders, N., Rakovec, O., Pan, M., Zink, M., Sheffield, J., Wood, E.F., Marx, A.,  
687 2018. Anthropogenic warming exacerbates European soil moisture droughts. *Nature Climate Change* 8, 421–426. URL:  
688 <https://www.nature.com/articles/s41558-018-0138-5>, doi:10.1038/s41558-018-0138-5.

- 692 Sen, P.K., 1968. Estimates of the Regression Coefficient Based on Kendall's Tau. *Journal of the American Statistical Association*  
 693 63, 1379–1389. URL: <http://www.tandfonline.com/doi/abs/10.1080/01621459.1968.10480934>, doi:[10.1080/01621459.1968.10480934](https://doi.org/10.1080/01621459.1968.10480934).
- 694 Senf, C., Buras, A., Zang, C.S., Rammig, A., Seidl, R., 2020. Excess forest mortality is consistently linked to drought  
 695 across Europe. *Nature Communications* 11, 6200. URL: <https://www.nature.com/articles/s41467-020-19924-1>, doi:[10.1038/s41467-020-19924-1](https://doi.org/10.1038/s41467-020-19924-1).
- 696 Slette, I.J., Post, A.K., Awad, M., Even, T., Punzalan, A., Williams, S., Smith, M.D., Knapp, A.K., 2019. How ecologists  
 697 define drought, and why we should do better. *Global Change Biology* 25, 3193–3200. URL: <https://onlinelibrary.wiley.com/doi/10.1111/gcb.14747>, doi:[10.1111/gcb.14747](https://doi.org/10.1111/gcb.14747).
- 698 Song, X.P., Hansen, M.C., Stehman, S.V., Potapov, P.V., Tyukavina, A., Vermote, E.F., Townshend, J.R., 2018. Global land  
 699 change from 1982 to 2016. *Nature* 560, 639–643. URL: <https://www.nature.com/articles/s41586-018-0411-9>, doi:[10.1038/s41586-018-0411-9](https://doi.org/10.1038/s41586-018-0411-9).
- 700 Souza, A.G.S.S., Ribeiro Neto, A., Souza, L.L.D., 2021. Soil moisture-based index for agricultural drought assessment: SMADI  
 701 application in Pernambuco State-Brazil. *Remote Sensing of Environment* 252, 112124. URL: <https://linkinghub.elsevier.com/retrieve/pii/S0034425720304971>, doi:[10.1016/j.rse.2020.112124](https://doi.org/10.1016/j.rse.2020.112124).
- 702 Taucare, M., Viguier, B., Figueira, R., Daniele, L., 2024. The alarming state of Central Chile's groundwater resources: A  
 703 paradigmatic case of a lasting overexploitation. *Science of The Total Environment* 906, 167723. URL: <https://linkinghub.elsevier.com/retrieve/pii/S0048969723063507>, doi:[10.1016/j.scitotenv.2023.167723](https://doi.org/10.1016/j.scitotenv.2023.167723).
- 704 Tennekes, M., 2018. tmap: Thematic Maps in R. *Journal of Statistical Software* 84, 1–39. doi:[10.18637/jss.v084.i06](https://doi.org/10.18637/jss.v084.i06).
- 705 Urrutia-Jalabert, R., González, M.E., González-Reyes, A., Lara, A., Garreaud, R., 2018. Climate variability and forest fires in  
 706 central and south-central Chile. *Ecosphere* 9, e02171. URL: <https://esajournals.onlinelibrary.wiley.com/doi/10.1002/ecs2.2171>, doi:[10.1002/ecs2.2171](https://doi.org/10.1002/ecs2.2171).
- 707 Van Loon, A.F., Gleeson, T., Clark, J., Van Dijk, A.I., Stahl, K., Hannaford, J., Di Baldassarre, G., Teuling, A.J., Tallaksen,  
 708 L.M., Uijlenhoet, R., Hannah, D.M., Sheffeld, J., Svoboda, M., Verbeiren, B., Wagener, T., Rangecroft, S., Wanders, N.,  
 709 Van Lanen, H.A., 2016. Drought in the Anthropocene. *Nature Geoscience* 9, 89–91. doi:[10.1038/ngeo2646](https://doi.org/10.1038/ngeo2646).
- 710 Venegas-González, A., Juñent, F.R., Gutiérrez, A.G., Filho, M.T., 2018. Recent radial growth decline in response to increased  
 711 drought conditions in the northernmost Nothofagus populations from South America. *Forest Ecology and Management* 409,  
 712 94–104. URL: <https://linkinghub.elsevier.com/retrieve/pii/S0378112717313993>, doi:[10.1016/j.foreco.2017.11.006](https://doi.org/10.1016/j.foreco.2017.11.006).
- 713 Venegas-González, A., Muñoz, A.A., Carpintero-Gibson, S., González-Reyes, A., Schneider, I., Gipolou-Zuñiga, T., Aguilera-  
 714 Betti, I., Roig, F.A., 2023. Sclerophyllous Forest Tree Growth Under the Influence of a Historic Megadrought in the  
 715 Mediterranean Ecoregion of Chile. *Ecosystems* 26, 344–361. URL: <https://link.springer.com/10.1007/s10021-022-00760-x>,  
 716 doi:[10.1007/s10021-022-00760-x](https://doi.org/10.1007/s10021-022-00760-x).
- 717 Vicente-Serrano, S.M., Azorin-Molina, C., Sanchez-Lorenzo, A., Revuelto, J., López-Moreno, J.I., González-Hidalgo, J.C.,  
 718 Moran-Tejeda, E., Espejo, F., 2014. Reference evapotranspiration variability and trends in Spain, 1961–2011. *Global  
 719 and Planetary Change* 121, 26–40. URL: <https://linkinghub.elsevier.com/retrieve/pii/S0921818114001180>, doi:[10.1016/j.gloplacha.2014.06.005](https://doi.org/10.1016/j.gloplacha.2014.06.005).
- 720 Vicente-Serrano, S.M., Beguería, S., López-Moreno, J.I., 2010. A multiscalar drought index sensitive to global warming: The  
 721 standardized precipitation evapotranspiration index. *Journal of Climate* 23, 1696–1718. URL: <http://dx.doi.org/10.1175/2009JCLI2909.1>, doi:[10.1175/2009JCLI2909.1](https://doi.org/10.1175/2009JCLI2909.1).
- 722 Vicente-Serrano, S.M., Peña-Angulo, D., Beguería, S., Domínguez-Castro, F., Tomás-Burguera, M., Noguera, I., Gimeno-  
 723 Sotelo, L., El Kenawy, A., 2022. Global drought trends and future projections. *Philosophical Transactions of the Royal  
 724 Society A: Mathematical, Physical and Engineering Sciences* 380, 20210285. URL: <https://royalsocietypublishing.org/doi/10.1098/rsta.2021.0285>, doi:[10.1098/rsta.2021.0285](https://doi.org/10.1098/rsta.2021.0285).
- 725 Vicente-Serrano, S.M., McVicar, T.R., Miralles, D.G., Yang, Y., Tomas-Burguera, M., 2020. Unraveling the influence of  
 726 atmospheric evaporative demand on drought and its response to climate change. *WIREs Climate Change* 11, e632. URL:  
 727 <https://wires.onlinelibrary.wiley.com/doi/10.1002/wcc.632>, doi:[10.1002/wcc.632](https://doi.org/10.1002/wcc.632).
- 728 Wickham, H., Averick, M., Bryan, J., Chang, W., McGowan, L.D., François, R., Grolemund, G., Hayes, A., Henry, L., Hester,  
 729 J., Kuhn, M., Pedersen, T.L., Miller, E., Bache, S.M., Müller, K., Ooms, J., Robinson, D., Seidel, D.P., Spinu, V., Takahashi,  
 730 K., Vaughan, D., Wilke, C., Woo, K., Yutani, H., 2019. Welcome to the tidyverse. *Journal of Open Source Software* 4, 1686.  
 731 doi:[10.21105/joss.01686](https://doi.org/10.21105/joss.01686).
- 732 Wilhite, D.A., Glantz, M.H., 1985. Understanding: The drought phenomenon: The role of definitions. *Water International* 10,  
 733 111–120. URL: <http://dx.doi.org/10.1080/02508068508686328>, doi:[10.1080/02508068508686328](https://doi.org/10.1080/02508068508686328).
- 734 Wilks, D.S., 2011. Empirical distributions and exploratory data analysis. *Statistical Methods in the Atmospheric Sciences* 100.
- 735 Winkler, K., Fuchs, R., Rounsevell, M., Herold, M., 2021. Global land use changes are four times greater than previously  
 736 estimated. *Nature Communications* 12, 2501. URL: <https://www.nature.com/articles/s41467-021-22702-2>, doi:[10.1038/s41467-021-22702-2](https://doi.org/10.1038/s41467-021-22702-2).
- 737 WMO, Svoboda, M., Hayes, M., Wood, D.A., 2012. Standardized Precipitation Index User Guide. WMO, Geneva. URL:  
 738 [http://library.wmo.int/opac/index.php?lvl=notice\\_display&id=13682](http://library.wmo.int/opac/index.php?lvl=notice_display&id=13682). series Title: WMO Publication Title: WMO-No.  
 739 1090 © Issue: 1090.
- 740 Wright, M.N., Ziegler, A., 2017. ranger: A Fast Implementation of Random Forests for High Dimensional Data in C++ and  
 741 R. *Journal of Statistical Software* 77, 1–17. doi:[10.18637/jss.v077.i01](https://doi.org/10.18637/jss.v077.i01).
- 742 Wu, C., Zhong, L., Yeh, P.J.F., Gong, Z., Lv, W., Chen, B., Zhou, J., Li, J., Wang, S., 2024. An evaluation framework  
 743 for quantifying vegetation loss and recovery in response to meteorological drought based on SPEI and NDVI. *Science of  
 744 The Total Environment* 906, 167632. URL: <https://linkinghub.elsevier.com/retrieve/pii/S0048969723062599>, doi:[10.1016/j.scitotenv.2023.167632](https://doi.org/10.1016/j.scitotenv.2023.167632).

- 757 Xiao, C., Zaehle, S., Yang, H., Wigneron, J.P., Schmullius, C., Bastos, A., 2023. Land cover and management effects on  
758 ecosystem resistance to drought stress. *Earth System Dynamics* 14, 1211–1237. URL: <https://esd.copernicus.org/articles/14/1211/2023/>, doi:[10.5194/esd-14-1211-2023](https://doi.org/10.5194/esd-14-1211-2023).
- 760 Yang, J., Huang, X., 2021. The 30 m annual land cover dataset and its dynamics in China from 1990 to 2019. *Earth System  
761 Science Data* 13, 3907–3925. URL: <https://essd.copernicus.org/articles/13/3907/2021/>, doi:[10.5194/essd-13-3907-2021](https://doi.org/10.5194/essd-13-3907-2021).
- 762 Zambrano, F., 2023. Four decades of satellite data for agricultural drought monitoring throughout the growing season in Central  
763 Chile, in: Vijay P. Singh Deepak Jhajharia, R.M., Kumar, R. (Eds.), *Integrated Drought Management*, Two Volume Set.  
764 CRC Press, p. 28.
- 765 Zambrano, F., Lillo-Saavedra, M., Verbist, K., Lagos, O., 2016. Sixteen years of agricultural drought assessment of the  
766 biobío region in chile using a 250 m resolution vegetation condition index (VCI). *Remote Sensing* 8, 1–20. URL: <http://www.mdpi.com/2072-4292/8/6/530>, doi:[10.3390/rs8060530](https://doi.org/10.3390/rs8060530). publisher: Multidisciplinary Digital Publishing Institute.
- 768 Zambrano, F., Vrieling, A., Nelson, A., Meroni, M., Tadesse, T., 2018. Prediction of drought-induced reduction of agricultural  
769 productivity in Chile from MODIS, rainfall estimates, and climate oscillation indices. *Remote Sensing of Environment*  
770 219, 15–30. URL: <https://www.sciencedirect.com/science/article/pii/S0034425718304541>, doi:[10.1016/j.rse.2018.10.006](https://doi.org/10.1016/j.rse.2018.10.006).  
771 publisher: Elsevier.
- 772 Zambrano, F., Wardlow, B., Tadesse, T., Lillo-Saavedra, M., Lagos, O., 2017. Evaluating satellite-derived long-term historical  
773 precipitation datasets for drought monitoring in Chile. *Atmospheric Research* 186, 26–42. URL: <https://www.sciencedirect.com/science/article/pii/S0169809516305865>, doi:[10.1016/j.atmosres.2016.11.006](https://doi.org/10.1016/j.atmosres.2016.11.006). publisher: Elsevier.
- 774 Zhang, W., Wei, F., Horion, S., Fensholt, R., Forkel, M., Brandt, M., 2022. Global quantification of the bidirectional de-  
775 pendency between soil moisture and vegetation productivity. *Agricultural and Forest Meteorology* 313, 108735. URL:  
776 <https://linkinghub.elsevier.com/retrieve/pii/S0168192321004214>, doi:[10.1016/j.agrformet.2021.108735](https://doi.org/10.1016/j.agrformet.2021.108735).
- 777 Zhao, Y., Feng, D., Yu, L., Wang, X., Chen, Y., Bai, Y., Hernández, H.J., Galleguillos, M., Estades, C., Biging, G.S., Radke,  
778 J.D., Gong, P., 2016. Detailed dynamic land cover mapping of Chile: Accuracy improvement by integrating multi-temporal  
779 data. *Remote Sensing of Environment* 183, 170–185. URL: <https://linkinghub.elsevier.com/retrieve/pii/S0034425716302188>,  
780 doi:[10.1016/j.rse.2016.05.016](https://doi.org/10.1016/j.rse.2016.05.016).
- 782 Zhou, K., Li, J., Zhang, T., Kang, A., 2021. The use of combined soil moisture data to characterize agricultural drought  
783 conditions and the relationship among different drought types in China. *Agricultural Water Management* 243, 106479. URL:  
784 <https://linkinghub.elsevier.com/retrieve/pii/S0378377420305965>, doi:[10.1016/j.agwat.2020.106479](https://doi.org/10.1016/j.agwat.2020.106479).